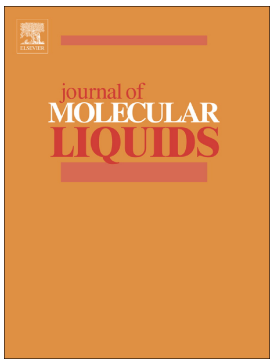

New 1-(Spiro[chroman-2,1′-cycloalkan]-4-yl)-1H-1,2,3-Triazoles: Synthesis, QTAIM/MEP analyses, and DNA/HSA-binding assays

Felipe S. Stefanello, Yuri G. Kappenberg, Alex Ketzer, Steffany F. Zorzin, Paulo R.S. Salbego, Thiago V. Acunha, Pablo A. Nogara, João B.T. Rocha, Marcos A.P. Martins, Nilo Zanatta, Bernardo A. Iglesias, Helio G. Bonacorso

PII: S0167-7322(20)36971-3

DOI: https://doi.org/10.1016/j.molliq.2020.114729

Reference: MOLLIQ 114729

To appear in: *Journal of Molecular Liquids*

Received date: 20 August 2020

Revised date: 1 October 2020

Accepted date: 5 November 2020

Please cite this article as: F.S. Stefanello, Y.G. Kappenberg, A. Ketzer, et al., New 1-(Spiro[chroman-2,1′-cycloalkan]-4-yl)-1H-1,2,3-Triazoles: Synthesis, QTAIM/MEP analyses, and DNA/HSA-binding assays, *Journal of Molecular Liquids* (2020), https://doi.org/10.1016/j.molliq.2020.114729

New 1-(Spiro[chroman-2,1'-cycloalkan]-4-yl)-1*H*-1,2,3-Triazoles: Synthesis, QTAIM/MEP Analyses, and DNA/HSA-Binding Assays

Felipe S. Stefanello[a], Yuri G. Kappenberg[a], Alex Ketzer[a], Steffany F. Zorzin[a], Paulo R. S. Salbego[a], Thiago V. Acunha[b], Pablo A. Nogara[c], João B. T. Rocha[c], Marcos A. P. Martins[a], Nilo Zanatta[a], Bernardo A. Iglesias[b,*] bernardopgq@gmail.com and Helio G. Bonacorso[a,*] helio.bonacorso@ufsm.br

[a]Núcleo de Química de Heterociclos (NUQUIMHE), Departamento de Química, Universidade Federal de Santa Maria, 97105-900 – Santa Maria, RS – Brazil.

[b]Laboratório de Bioinorgânica e Materiais Porfirínicos, Departamento de Química, Universidade Federal de Santa Maria, 97105-900 – Santa Maria, RS – Brazil.

[c] Departamento de Bioquímica e Biologia Molecular, Universidade Federal de Santa Maria, Santa Maria - RS, Brazil.

[*]Corresponding Authors.

Abstract

This study synthesized and characterized the DNA/HSA properties of a new series of 12 examples of 4-(alkyl/aryl)-1-(spiro[chroman-2,1'-cycloalkan]-4-yl)-1*H*-1,2,3-triazoles (SCTz), in which alkyl = $CH_3(CH_2)_5$ and aryl = C_6H_5, 4-$NH_2C_6H_4$, 3-$OCH_3C_6H_4$ (47-95% yield) by regioselective Copper-Catalyzed Azide–Alkyne Cycloaddition (CuAAC) reaction. Additioanally, single crystal X-ray diffraction (SC-XRD) analysis was carried out and the SC-XRD data enabled a broad molecular analysis using QTAIM and MEP analysis. Absorption UV-Vis properties of SCTz series were investigated and all derivatives absorb in the UV region and no are observed emission fluorescence in solution. The DNA-binding assays (UV-Vis analysis) showed that the all spiro-derivatives demonstrated strong binding forces to CT-DNA. The Stern-Volmer quenching constants (K_{SV}) of SCTz were calculated and derivatives containing the OCH_3 group competed more strongly with DNA minor grooves, followed by the increasing general order of (K_{SV}): EB-DNA < DAPI-DNA. Additionally, the high values observed for the bimolecular quenching constant rate (k_q) indicated a static interaction between spiro-derivatives and DNA in all cases. Finally, the HSA-binding experiments and molecular docking studies for the new spiro-derivatives were

determined and quenching (K_{SV}) and quenching rate (k_q) constants values obtained for the SCTz suggest good interaction between HSA and derivatives, probably by static mechanism, forming HSA:compound adduct in the ground state.

Keywords*:* CuAAC reactions; Triazoles; DNA-Binding; HSA-binding.

Introduction

The 1,2,3-triazole is an important class of compounds that performs numerous biological activities and is widely used in organic synthesis, medicinal chemistry, and material science.[1–6] Molecules with this isomeric chemical compound are known to exhibit antimicrobial,[7] anti-HIV,[8] antitumoral,[9] anti-inflammatory,[10] antitubercular activities.[11,12]

Furthermore, it is well known that the chromenone framework is present in the synthetic components and a wide variety of natural compounds.[13–19] In this context, spirochromonones have attracted significant interest as a privileged structure in the development of several bioactive compounds with numerous biological activities.[20–28] [29–32] Recently, our research group showed that the use of spirochromones in cyclization with 2-aminobenzonitrile enables the production of tacrine hybrids. The tacrine hybrids synthesized in this method also presented moderate acetylcholinesterase (AChE) inhibitory effects.[22,33] Moreover, the same compounds were studied regarding the cytotoxic activity of tacrine derivates using glioblastoma cell line (SF295).[22]

Deoxyribonucleic acid is one of the main compositions of living organisms. The DNA biomacromolecule regulates many biochemical processes that occur in the cellular system. Therefore, understanding and investigating the interactions and mechanisms of biological-target molecules binding with nucleic acids may be a more robust finding at the molecular level and particularly important for developing new drugs in the biological field.[34–36] In this context, it is necessary to design different compounds that may fit well in DNA binding (between nucleobases or by grooves), cleavage, and interactions with certain proteins, which is the main cellular target for anticancer derivatives. Investigating the interactions of molecules with human serum albumin (HSA) by spectroscopic methods provides important information on the binding or

interactions of a determined site.[37–39] As serum proteins perform transport, distribution, accumulation, and excretion properties of medical drugs in tumor tissues, special consideration must also be given to investigating the binding of spiro-derivatives to proteins.

In this manuscript, new triazole systems bounded to benzopyrans with spiro carbons of 5, 6, and 7-membered rings (SCTz) are presented. The 1,2,3-triazole moiety is linked to the spirochromanes via click chemistry reaction, which allowed the production of a novel series of 4- (alkyl/aryl)-1-(spiro[chroman-2,1'-cycloalkan]-4-yl)-1*H*-1,2,3-triazoles (SCTz **10-13**) (Scheme 1). The efficiency of these new compounds and a variety of substituents on the spectroscopic and electrochemical behavior of the synthesized molecules was evaluated and the results presented and discussed. Additionally, DNA-binding, HSA-binding, and molecular docking analyses were conducted to better explain this biomolecule interaction type.

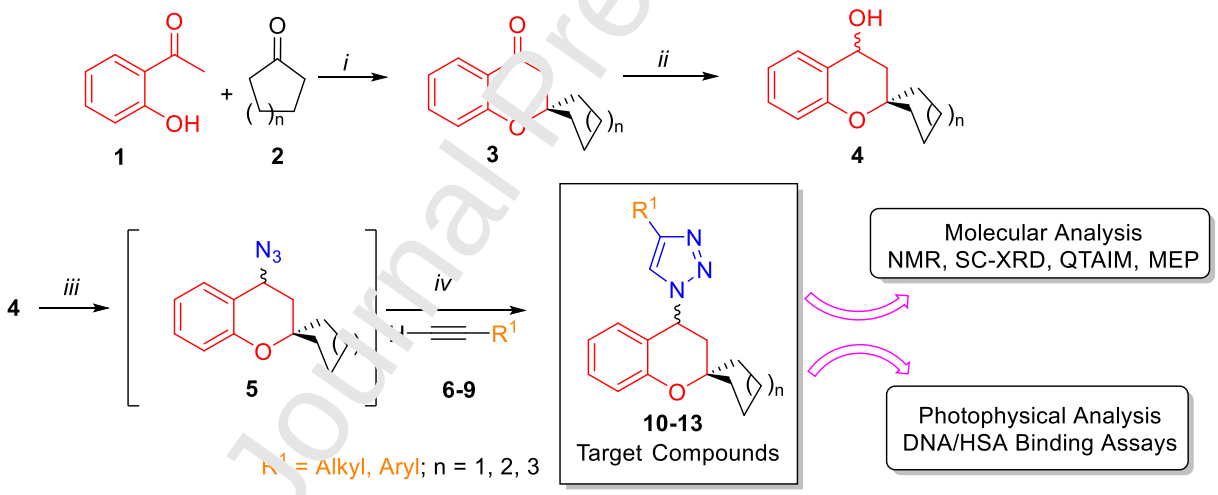

Scheme 1. Summary of this study. Reaction conditions: (i) Pyrrolidine; (ii) $NaBH_4$; (iii) (a) MsCl (b) NaN_3; (iv) CuAAC reaction.

Results and Discussion

Synthesis and characterization

The spiro[chromane-2,1'-cycloalkyl]-4-ones (**3a-c**) were prepared by adapting a common multi-component methodology developed by Kabbe et al.[31] and further

improved in the absence of solvent.[20,26] This resulted in a thermal condensation of 5-substituted-2-hydroxyacetophenones (**1a-c**) in the 5-position with cycloalkanones (**2a-c**) caused by the pyrrolidine, which produced the products in similar yields as described in the literature.[26]

Then, spirochromanones (**3a-c**) were converted to spirochroman-4-ols (**4a-c**) using sodium borohydride as the reducing agent in ethanol.[27] The products (**4a-c**) were obtained in the form of yellow, brown, and white viscous oils and white solids in yields of 67-85%, such as racemic mixtures with configuration 4*R*/4*S* and similar to those described in the literature,[27] and used in the synthesis of new 4-azidospiro[chroman-2,1'-cycloalkanes] (**5a-c**) without isolation (Scheme 2).

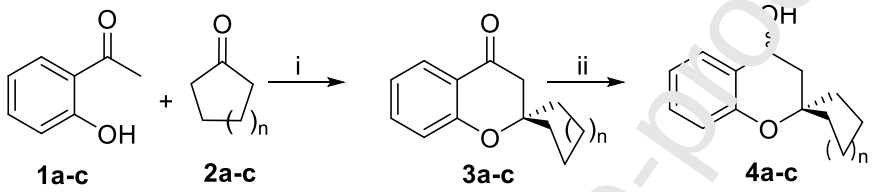

Compds **1-4**: **a** (n=1), **b** (n=2), **c** (n=3)

Scheme 2. Synthesis of spirochroman-4-ols. Reaction conditions: (i) Pyrrolidine, 110 ºC, 6 h; (ii) $NaBH_4$, EtOH, 80 ºC, 1h (67-85%).

The series of compounds (**5a-c**) were obtained from a nucleophilic substitution reaction. For this, spirochroman-4-ols (**4a-c**) and mesyl chloride were used as they lead to the formation of spiro[chroman-1'-cycloalkan]-4-yl methanesulfanates, followed by a substitution reaction with sodium azide in order to form organic azides **5**. The obtained products were yellow oils and used in the next step also without purification (Scheme 3). From the 4-azidospiro[chroman-2,1'-cycloalkanes] (**5a-c**), it was then possible to obtain a series of SCTz (**10-13**) via CuAAC reaction.

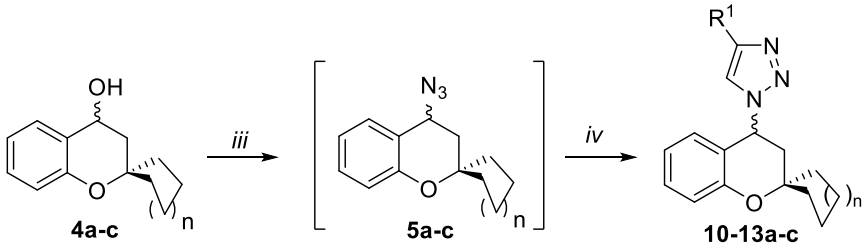

R^1/(Compd.): C_6H_5 (**10**), 4-$NH_2C_6H_4$(**11**) 3-$OCH_3C_6H_4$(**12**), $(CH_2)_5CH_3$(**13**)
Compds **4, 5, 10-13**: **a** (n=1), **b** (n=2), **c** (n=3).

Scheme 3. Synthesis of 4-(alkyl/aryl)-1-(spiro[chroman-2,1'-cycloalkan]-4-yl)-1*H*-1,2,3-triazoles. Reaction conditions: (iii) (a) **4a-c** (1 eq), MsCl (4 eq), CH_2Cl_2 dry, 0 ºC, 15 min; (b) NaN_3 (2.5 eq), DMF, 80 ºC, 12h. (iv) Terminal alkynes, sodium ascorbate (10 mol%)/$CuSO_4.5H_2O$ (20 mol%), THF/H_2O (1:1), room temperature, 24 h (47-95% yield).

Firstly, in order to obtain the triazole **10b** as the target, a methodology previously described by the NUQUIMHE group[26] was tested, starting with **5b**. Employing the conditions previously described,[26] factors such as time, proportions of copper iodide, azide, and alkyne were optimized. The reaction conditions considered in the optimization process are shown in Table 1.

Table 1. Optimization of the reaction for the 1,2,3-triazole-spirochromane **10b.**

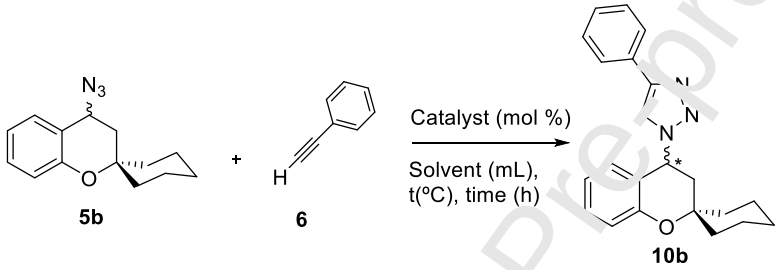

Entry	Catalyst (mol %)	Azide (5b) (mmol)	Alkyne (6) (mmol)	Solvent (v.v.v)	Temp (ºC)	Time (h)	Yield (10b) (%)
1	CuI (50)	1.5	1.0	THF/*t*-BuOH/H_2O 3:2:1 (2.5 mL)	80	12	5
2	CuI (25)	1.5	1.0	THF/*t*-BuOH/H_2O 3:2:1 (2.5 mL)	80	12	5
3	CuI (50)	1.5	1.0	THF/*t*-BuOH/H_2O 3:2:1 (2.5 mL)	80	24	16
4	CuI (50)	1.0	1.5	THF/*t*-BuOH/H_2O 3:2:1 (2.5 mL)	80	12	19
5	CuI (25)	1.0	1.5	THF/*t*-BuOH/H_2O 3:2:1 (2.5 mL)	80	12	24
6	CuI (25)	1.0	1.5	THF/*t*-BuOH/H_2O 3:2:1 (2.5 mL)	80	24	28
7	Cu source (20/20)	1.0	1.1	THF/H_2O 1:1 (5.0 mL)	25	24	66
8	Cu source (20/20)	1.0	1.5	THF/H_2O 1:1 (5.0 mL)	25	24	56

9	Cu source (20/20)	1.0	1.1	THF/H_2O 1:1 (5.0 mL)	65	24	66
10	Cu source (20/20)	1.0	1.1	t-BuOH/H_2O 1:1 (5.0 mL)	25	24	37
11	Cu source (30/30)	1.0	1.1	THF/H_2O 1:1 (5.0 mL)	25	24	46
12	Cu source (20/10)	1.0	1.1	THF/H_2O 1:1 (5.0 mL)	25	24	70
13	Cu source (30/10)	1.0	1.1	THF/H_2O 1:1 (5.0 mL)	25	24	47
14	Cu source (50/10)	1.0	1.1	THF/H_2O 1:1 (5.0 mL)	25	24	40

Cu source: $CuSO_4$. $5H_2O$) : NaAsc (mol%). NaAsc = Sodium Ascorbate.

In entry 1, the reaction conditions previously described by Ketzer et al.[26] were reproduced for this system. In entries 2-6, some parameters were changed in order to increase the yield of the triazole, such as decreasing the concentration of copper(I) iodide,[40] the reaction time, the proportions of the azide, and the terminal alkyne, although there was no change in the yield.

Lastly, copper iodide as a catalyst for click chemistry reactions was not considered satisfactory due to the low yields obtained. This is because the catalyst used may have formed oxidative coupling products.[5] Another disadvantage of using Cu(I) salts is their thermodynamic instability, which can be oxidized to Cu(II) and/or disproportionate to copper and Cu(II) in the course of the reaction.[29]

Therefore, another strategy was used to obtain SCTz (**10a-c**), (**11a-c**), (**12a-c**), and (**13a-c**), as it was observed in the literature[11] that heterocycles similar to those proposed here used a different copper source than the one previously tested. Thus, copper sulfate pentahydrate combined with sodium ascorbate was used and the catalyst prepared in situ by reducing Cu (II) salts. Ascorbic acid or sodium ascorbate proved to be excellent reducing agents to prepare several 1,4-triazoles in high yields and purity.[4,6] According to the literature, a small excess of reducing agent is generally added to prevent the formation of oxidative coupling products, which are often observed when a source of Cu(I) is added directly.[5] The preparation of 1,2,3-triazoles-1,4-disubstituted was carried out, on average, from 6 to 36 h at room temperature.

In entry 7, the reaction conditions previously described by Sajja[11] were reproduced and generated a yield of 66% of the final product. During this reaction

condition, we sought to improve the yield of the final product (**10b**) by varying its reaction conditions. The variation of the proportion of alkyne of entries 8 and 9 were initially studied by increasing their quantity of azide and temperatures, respectively, while maintaing the other paramaters the same, resulting in a smaller yield for entry 7.[9] Many methodologies[6] report the use of solvent mixtures in the reactions, such as tetrahydrofuran and water or tert-butanol and water, although these variations of the reaction solvent proved to be inefficient in entry 10. After establishing that the conditions of entry 7 were even more efficient, they varied for proportions of sodium ascorbate and copper sulfate pentahydrate[30] in entries 11-14. Thus, it can be noted that the increased proportions of the catalysts proved ineffective for entry 11. Furthermore, the proportions of sodium ascorbate relative to copper sulfate pentahydrate varied in entries 12, 13, and 14, showing that as the proportion of sodium ascorbate increased, the yield also decreased proportionally.

In this way, it was possible to observe that entry 12 was the most efficient form to obtain the triazole **10b**, which was extended and used to synthesize the series SCTz (**10a-c**), (**11a-c**), (**12a-c**), (**13a-c**), and yields ranging from 47 to 95%. The SCTz (**10a-c**), (**11a-c**), (**12a-c**), and (**13a-c**) were characterized by NMR experiments. Depending on the compound, gas chromatography coupled to mass spectrometry (GC/MS), high-resolution mass spectrometry (LC-HRMS) or both were performed. Moreover, it was possible to characterize some compounds by the crystal structure (SC-XRD).

No major differences in the NMR spectra were observed through the compound series (**10**, **11**, **12**, and **13**), which is mainly due to the nature of the spiro substituents. Therefore, **10b** will be used as an example for the proper signal assignment. In the ^{1}H NMR spectrum performed on 400 MHz, in $CDCl_3$ as solvent for triazole **10b** (see *Supporting Information*, Fig. S15), it was possible to observe the signals of the hydrogens of the phenyl in the aromatic region in which the most disjointed ones were H-4c/H-4c', appearing in the form of a doublet in δ 7.83 ppm with $^{1}J_{HH}$ = 7 Hz. Then, the aromatic H-4b/H-4b' hydrogens appeared in the aromatic region as the multiplet δ 7.46-7.37 ppm and H-4d appeared as a triplet at δ 7.33 ppm $^{1}J_{HH}$ = 7.5 Hz and also hydrogen H-5 (triazole ring) appears as a singlet at δ 7.66 ppm.The two aromatic hydrogens relative to the chromane moiety are in the form of multiplets at δ 7.31-7.21 ppm for H-7 and 7.01-6.94 ppm for H-5. The other two H-6 and H-8 aromatic

hydrogens are in oxygen shielding zones (O1) and were overlapped at δ 6.90- 6.80 ppm in the form of a multiplet.

It was also possible to observe a doublet of doublets at δ 6.14 ppm with $^{1}J_{HH}$ = 11.5 Hz and $^{2}J_{HH}$ = 6.5 Hz referring to the H-4 of spirochromane moiety. The multiplicity of H-4 is present due to the interaction with the diastereopic hydrogens H-3a and H-3a, which are doublets of doublets in the 2.52 ppm and 2.29 ppm regions with $^{1}J_{HH}$ = 13 Hz and $^{2}J_{HH}$ = 6.5 Hz and $^{1}J_{HH}$ = 13 Hz and $^{2}J_{HH}$ = 11.5 Hz, respectively. The multiplet at δ 1.99-1.37 ppm refers to signals from the ten diastereotopic hydrogens that make up the spirocarbocyclic moiety.

For the ^{13}C NMR spectrum was performed on 100 MHz in $CDCl_3$ as solvent for compound **10b** (see *Supporting Information*, Fig. S16). The signal of the C-8a quaternary carbon was bound to the chromane oxygen at δ 153.6 ppm and C-4a for the triazole ring at δ 148.3 ppm. The aromatics bound to C-4, C-4c/C-4c', C-4d, C-4b/C-4b', and C-5 of triazole are shown in δ 130.6, 128.8, 128.1, 125.7, and δ 117.8 ppm, respectively. Signals of the chromane ring C-7, C-8, C-6, C-4a, and C-5 aromatic carbons appear at δ 130.1, 127.5, 120.7, 119.2, and δ 118.0 ppm, respectively. The signal for C-2 appears almost superimposed on $CDCl_3$ at δ 76.1 ppm. Spiro carbon C-4 exhibited chemical shifts at δ 54.2 ppm and C-3 showed a higher field signal at δ 40.1 ppm. The signals relating to C-2', C-3', C-4', C-5', and C-6' of the spirocarbocyclic moiety appeared in the range δ 37.8 – 21.5 ppm.

Molecular Insights

Single crystal X-ray diffraction (SC-XRD) analysis was carried out to confirm the molecular structure of the obtained the SCTz series of compounds in the solid state. Additional structures were obtained to furnish molecular insights on the influence of different substituents in these novel structures. Complete crystallographic data and molecular diagrams are shown in the *Supporting Information* - Table S1, Fig. S1 for compounds **10b**, **11b**, **12b-c**, and **13c**. A racemic mixture was observed in the crystalline solid state in all obtained structures.

From the molecular overlay and by using the triazole as reference, it is possible to observe qualitatively the two main torsion angles that occur in these models in all five structures (Table 2). Torsion angle φ_1 changed and ranged from 17.41 to 30.5° in

absolute values for **10b**, **11b**, and **12b-c**. The highest difference occurred by the presence of the MeO substituent (**12b**) compared with **10b** (around 12°). The addition of one carbon to the spiro portion in **12c** did not affect torsion angle φ_1 when compared with **12b**, although it significantly affected torsion angle φ_2. The addition of the alkyl chain in R^1 (**13c**) echoed in the molecule, affecting the value of torsion angle φ_2 and overlapping the additional carbon in the spiro portion.

Table 2. Angle between planes (θ), torsion angles (ϕ), and molecular overlay[a] of the obtained crystalline structures.

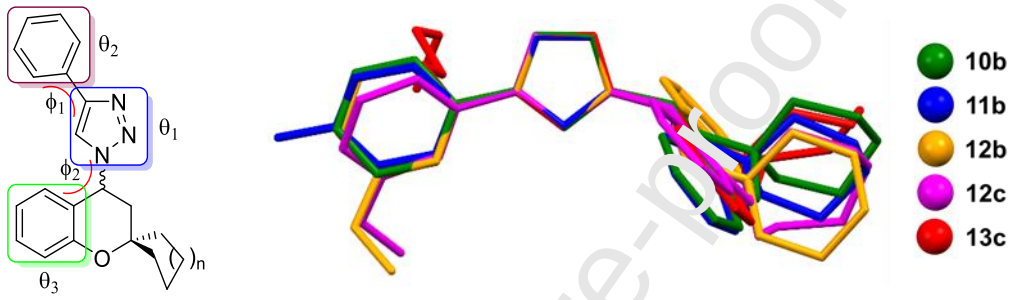

Structure	Torsion Angles (ϕ)[b]		Angle Between Planes (θ)	
	ϕ_1 (°)	ϕ_2 (°)	θ_1 vs θ_2 (°)	θ_1 vs θ_3 (°)
10b	17.41	-62.59	18.65	81.65
11b	-19.51	-64.32	20.23	82.30
12b	29.37	72.96	28.74	87.95
12c	-30.51	-79.40	31.21	88.98
13c	-125.72	-71.90	84.27[d]	88.07

[a]Molecular overlay using triazole atoms (N1-N2-N3-C11-C10). [b]ϕ_1: C17-C12-C11-C10; ϕ_2: C4-C3-N1-C10. [c]ϕ_1: C13-C12-C11-C10. [d]Alkyl portion (C12-C13-C14-C15-C16-C17) used for plane θ_2.

The angles between planes (θ) were calculated to observe the geometric influence of the substituents on the molecular structure (Table 2). The angle values between planes θ_1 and θ_2 increased through the different substituents. These changes are likely due to the higher influence of the intermolecular environment, that is, the result of the intermolecular interactions with the neighboring molecules. Compound **13c** is a good example of this intermolecular influence, as it showed a value of almost 90° between the planes. This may have occurred because of the topology adjustment of the alkyl chain to achieve higher complementarity and energetic stabilization. The values

between θ_1 and θ_3 were similar and ranged from 81.65 to 88.98°, which probably due to a subtle intermolecular influence and another consequence of molecular changes.

This geometric discussion (Table 2) provides a superficial analysis of the nature of these models. Additionally, this geometric approach (distances and/or angles between atoms or planes) can sometimes result in misleading interpretations, especially when dealing with 'weaker' interactions, as already reported.[41] Therefore, a broader molecular analysis of the context of intramolecular interactions must be performed.

Quantum Theory of Atoms in Molecules (QTAIM) analysis was performed in order to better understand these models in an intramolecular interaction context. The QTAIM provides a quantum description of the location and behavior of the atoms in a chemical bond.[42] It also furnishes the electron density (ρ) of each bond critical point (BCP), which is the minimum electron density of/in the bond path.[42] From these data, the interaction between atoms is obtained by the BCP and may provide additional information on the nature of the interactions and description of the chemical bond and interactions.[43]

Nevertheless, only compound **10b** showed some interaction (Figure 1), which was revealed by C-H···H-C intramolecular interactions between the hydrogen atom of the chromane portion (atoms C3-H3) and a hydrogen atom from the spyro portion (atoms C22-H22B). The observed C-H···H-C interaction presented a considerable H_{BCP} (V/2) value of -2.82 kcal mol^{-1}. The molecular QTAIM analysis for structures **11b**, **12b-c**, and **13c** are described in the ESI.

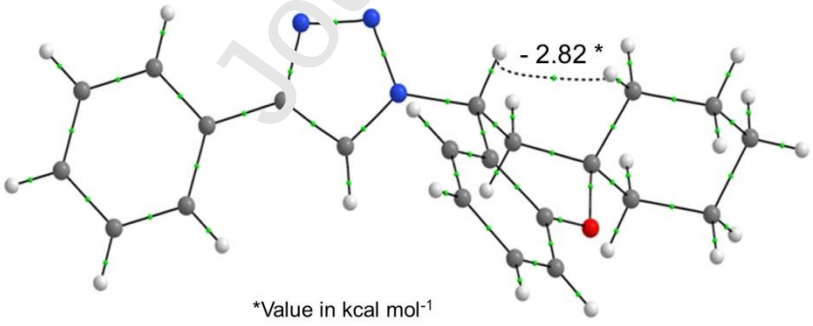

Figure 1. BCP of the intramolecular interaction observed by QTAIM for compound **10b**.

Molecular electrostatic potential analysis (MEP)[44,45] was performed in order to obtain information on the main molecular regions in which these structures interact, either by self-assembly or possible molecular docking (Figure 2). This analysis furnishes regions with negative and positive electrostatic potential in the considered

molecule.[44,45] The MEPs of compounds **10b**, **11b**, **12b-c**, and **13c**, with their values of higher potential regions highlighted, are illustrated in Figure 2.

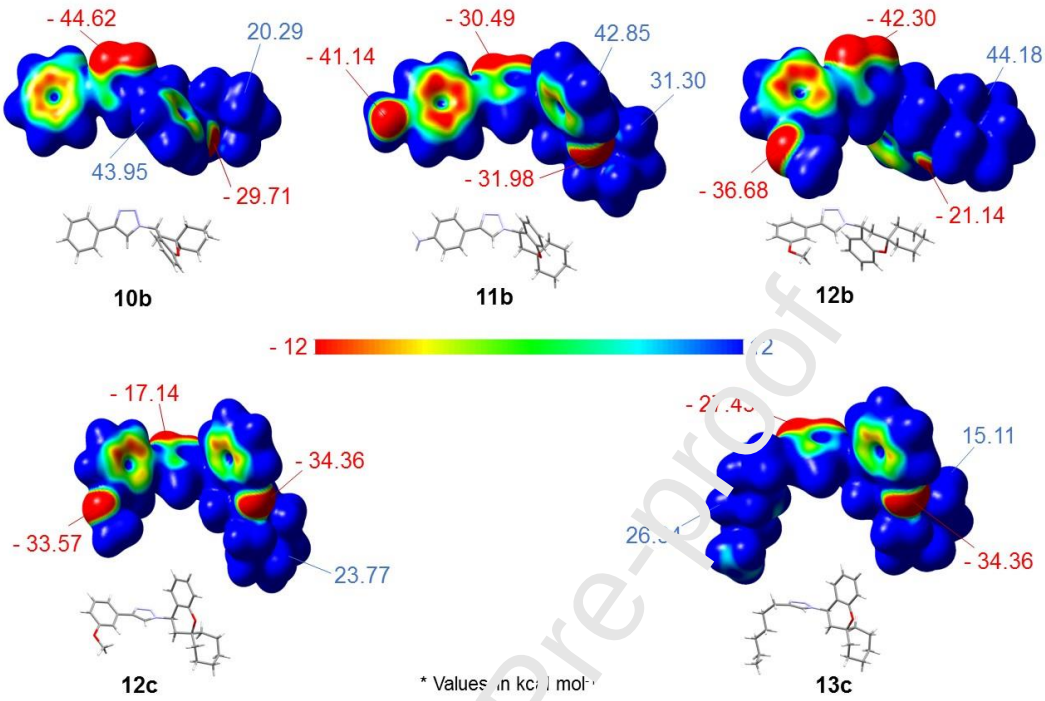

Figure 2. Molecular electrostatic potential (MEP) maps of SCTz **10b**, **11b**, **12b-c**, and **13c**.

In general, the structures showed increased negative regions in the nitrogen atoms of the triazole that may be involved in intermolecular interactions (binding) (Figure 2). The analysis also showed the expected negative regions of the oxygen and nitrogen atoms of CH_3O (**12b-c**) and NH_2 (**13c**) substituents, respectively. Moreover, it is possible to observe a considerable portion of the molecule with positive regions, especially the spiro portion. Aditionally, compound **13c** presented a 'blue wall' of positive electrostatic potential region of the hydrogen atoms from the alkyl portion (Figure 2). This portion may be important in the intermolecular context, complementarity between molecules or binding situations, to best accommodate the components.

The atoms involved in the observed C-H···H-C intramolecular interaction (Figure 1) in compound **10b** did not demonstrate complementarity of electrostatic potential regions in the MEP analysis (see *Supporting Information*, Fig. S2). This indicates that this intramolecular interaction occurred due to high proximity between the hydrogen atoms, which is the result of its molecular topology and likely caused by the intermolecular environment.

Absorption analysis by UV-Vis spectroscopy

The comparative UV-Vis absorption spectra of the compounds using dimethyl sulfoxide (DMSO) as solvent are shown in Figure 3 and the absorption properties are listed in Table 3. All SCTz showed absorption maxima around the 250–450 nm range in the ultraviolet region. The values for the molar absorptivity coefficient (ε) for these compounds indicated that spin and symmetry allowed electronic transitions, which may be related to π→π* transitions (Figure 3a-c). Slightly changes were osberved in the absorption maxima location or wavelength shift associated with the different stereochemistry in the SCTz. Moreover, for all spiro-derivatives, no fluorescence emission in DMSO solution was observed.

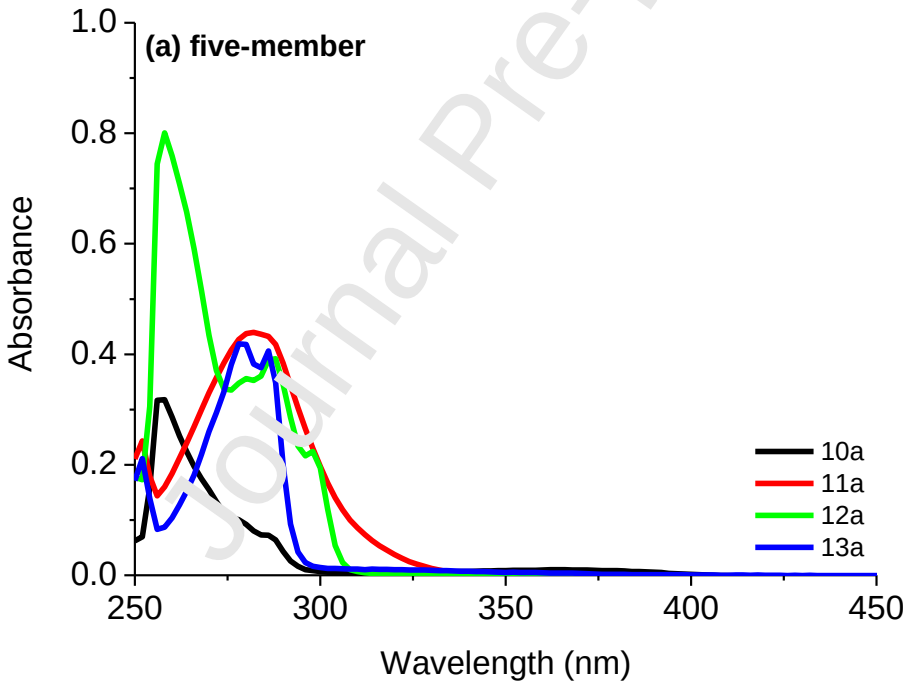

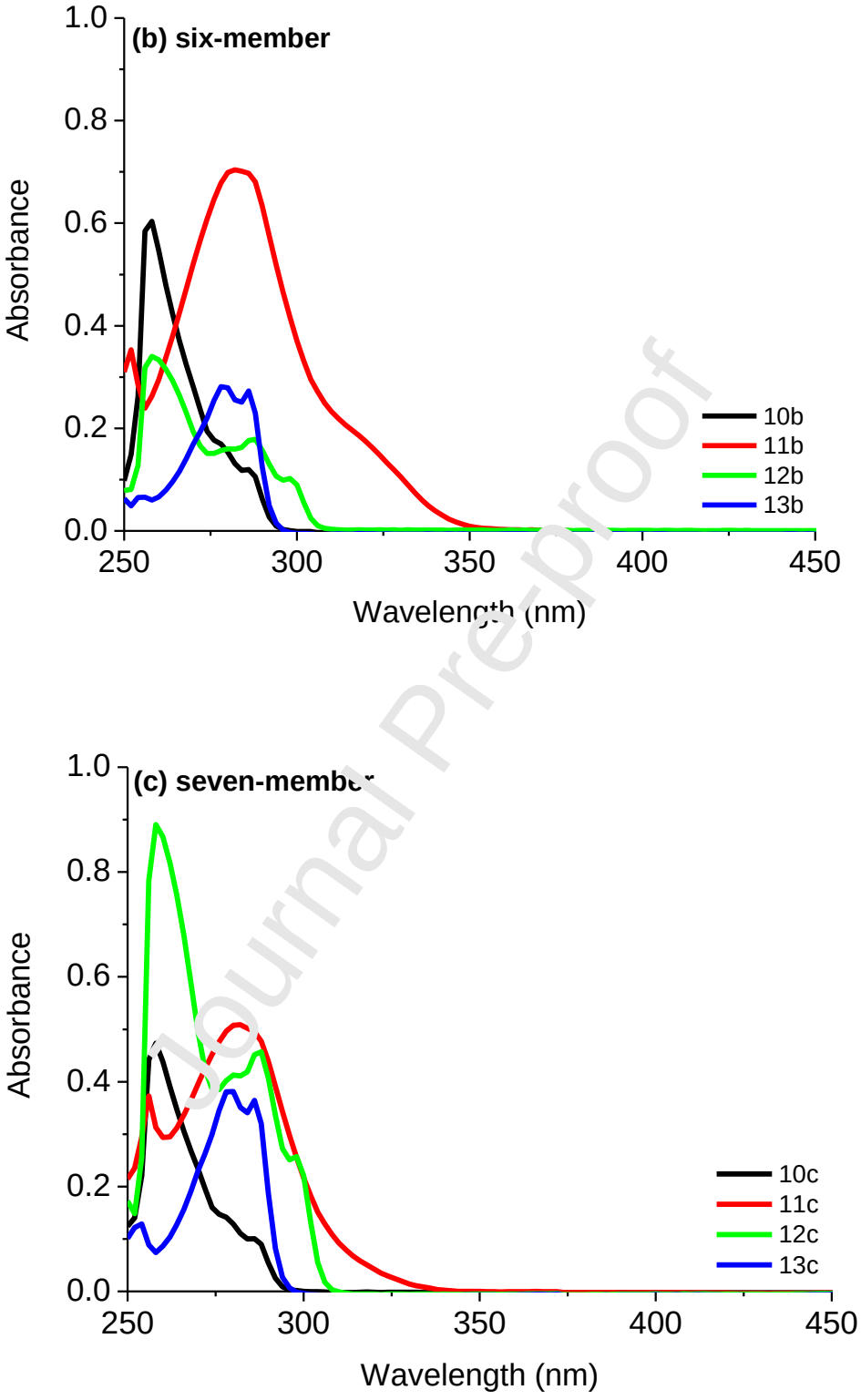

Figure 3. Electronic UV–Vis absorption spectra of SCTz containing different structures **(a)** five-member, **(b)** six-member and **(c)** seven-member spiro-ring, all in DMSO solutions ([ ] = 1.2 – 1.35 x 10^{-4} M).

Table 3. Absoption UV-Vis transitions values of SCTz.

Derivative	λ, nm (ε; M^{-1} cm^{-1})
10a	257 (2,641); 366 (bb)*
10b	258 (4,808); 286 (sh)**
10c	258 (3,900)
11a	282 (3,658)
11b	283 (5,192)
11c	256 (2,968); 281 (4,072)
12a	258 (6,115); 288 (2,992); 298 (sh)**
12b	258 (2,816); 288 (1,491); 298 (850)
12c	259 (6,245); 288 (3,010); 298 (sh)**
13a	278 (3,360); 286 (3,240)
13b	278 (2,341); 286 (2,250)
13c	279 (3,211); 285 (3,052)

*Broad band; **Shoulder.

DNA-binding assays by UV-Vis analysis

The interaction of SCTz series with CT-DNA was also studied by absorption UV-vis spectroscopy at the 250–600 nm range in DMSO (2%)/Tris-HCl buffer solution (pH 7.4). The SCTz interact with CT-DNA and give a transition band change in the ultraviolet range. The effects of different concentrations of CT-DNA on the electronic absorption spectra of the compounds are presented in Figure 4. Generally, as DNA concentrations increased, the SCTz had characteristic changes (hyperchromicity and bathochromic shift) in the absorption electronic spectra (Table 4).

The addition of various concentrations of CT-DNA (0 to 100 μM) increased absorbance in the $\pi \rightarrow \pi^*$ transition band at the ultraviolet range. Blue or red-shifts were observed depending on the substituent, which is an indication of possible intercalation modes of the spiro molecules between DNA nitrogeneous base pairs (e.g. compound **10a**; Figure 4).[32] The other interactive possibility of these derivatives is probably H-bonding forces with the DNA bases or the presence of the triazole moiety in the structure that may interact with DNA bases via covalent interactions, as previously reported for other triazoles derivatives.[46–48]

Moreover, the intrinsic binding constants (K_b) of the SCTz were calculated (Table 4). In general, all 1,2,3-triazoles derivatives demonstrated strong binding forces to CT-DNA ($K_b \approx 10^6$ M^{-1}) following the increasing order of K_b values: **12c** < **13c** < **11a** <

10b < **10a** ≈ **13a** < **13b** < **11c** < **10c** < **12b** < **11b** < **12a**. The CT-DNA UV-vis titration spectra of all derivatives are listed in *Supporting Information* (Figs. S60–S70).

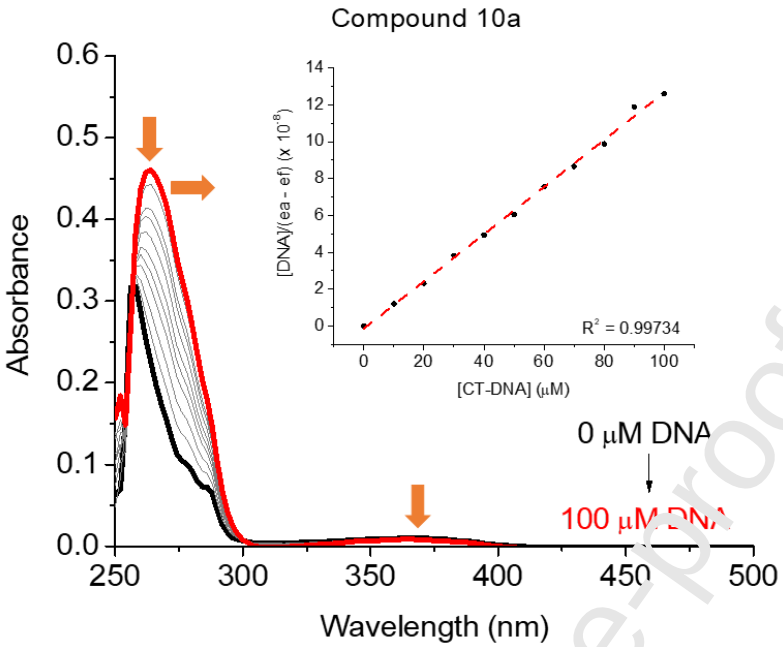

Figure 4. UV-Vis titration absorption spectra of derivative **10a** in a DMSO (2%)/Tris-HCl buffer (pH 7.4) mixture. The concentration of CT-DNA ranged from 0 to 100 μM. *Insert graph*: plot of [DNA]/(εa – εf) vs. [DNA].

Table 4. CT-DNA-binding results by UV-Vis absorption analysis for the SCTz series.

Derivative	***H*%**[a]	**Δλ (nm)**[b]	**K_b (M^{-1})**[c]	**ΔG° (kcal mol^{-1})**
10a	30.90	6.0	1.00 x 10^6	−8.18
10b	22.55	4.0	0.94 x 10^6	−8.14
10c	33.50	4.0	1.28 x 10^6	−8.32
11a	39.90	9.0	0.77 x 10^6	−8.02
11b	25.60	7.0	1.86 x 10^6	−8.55
11c	34.20	8.0	1.09 x 10^6	−8.23
12a	19.50	4.0	3.70 x 10^6	−8.95
12b	44.70	6.0	1.80 x 10^6	−8.53
12c	11.45	4.0	0.66 x 10^6	−7.93
13a	38.60	1.0	1.02 x 10^6	−8.19
13b	49.20	3.0	1.05 x 10^6	−8.21
13c	38.00	1.0	0.70 x 10^6	−7.97

[a]Hyperchromicity of Soret band: $H(\%) = (Abs_{initial} – Abs_{final}) / (Abs_{initial}) \times 100$;

[b]Red shift: $\Delta\lambda = \lambda_{initial} – \lambda_{final}$;

[c]Binding constant by absorption UV-Vis analysis.

Dye-DNA competition assays by steady-state fluorescence emission

Competitive-binding experiments using the quenching method to determine the displacement of the intercalating ethidium bromide (EB) or minor groove binder 4′,6-Diamidine-2′-phenylindole (DAPI) dyes from CT-DNA may provide further confirmation on the binding affinity of the complexes.

Emission spectra were monitored as increasing concentrations of SCTz series were added by titration to a fixed concentration of DNA pretreated with dyes (EB or DAPI). Interpretations of the changes observed in the dye spectra followed by binding to CT-DNA are often used for interaction studies between DNA and other compounds such as heterocyclic molecules.[49] The EB-DNA assays show strong emissions at 636 nm when excited at 510 nm (Figure 5). Moreover, Figure 5 also depicts the emission spectra of EB bound to CT-DNA in both the absence and presence of compound **10a**. When spiro-derivatives were added to the DNA pre-treated with EB, the nucleic acid-induced emission intensity of EB decreased (Figure 5). The results demonstrate a slight quenching of the fluorescence intensity of the EB-DNA complex followed by the addition of increasing concentrations of SCTz series, which may be attributed to the competition of spiro molecules with EB over binding to the grooves of DNA. The inset graphs in Figure 5 represent the Stern-Volmer plot, which was obtained as the relationship between F_0/F and [CT-DNA]. The EB-DNA emission spectra of the other spiro-derivatives are listed in *Supporting Information* (Figures S71-S81).

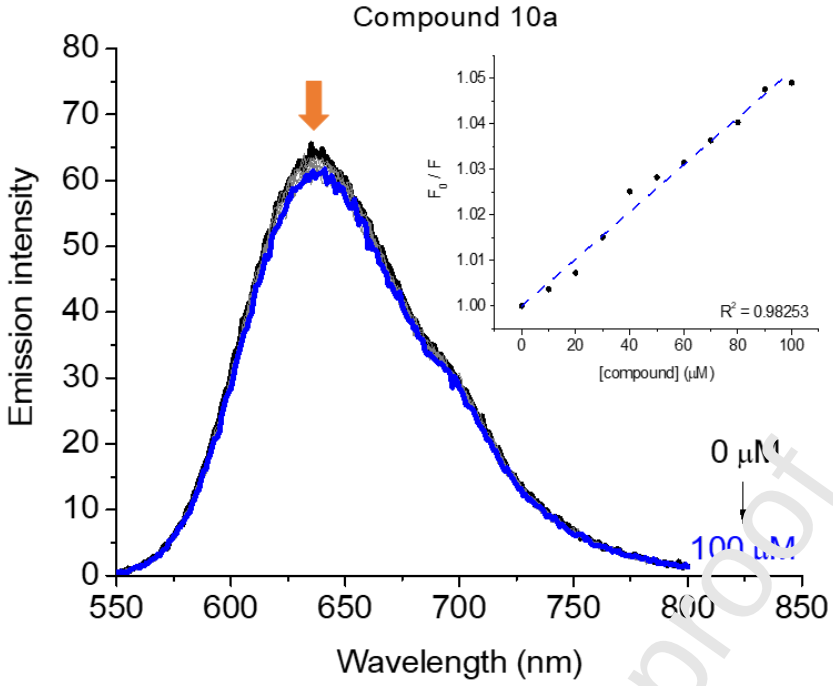

Figure 5. Steady-state emission fluorescence spectra of EB-DNA assays in the presence of compound **10a** in a DMSO (2%)/Tris-HCl buffer solution (pH 7.4), at λ_{exc} = 510 nm. The arrow indicates the changes in fluorescence at increasing concentrations of samples. *Insert graph*: plot of F_0/F *versus* [DNA].

In the next experiment, steady-state emission spectra were monitored as increasing concentrations of SCTz were added by the addition to a fixed concentration of CT-DNA pre-treated with DAPI dye as a minor groove binder molecule. The DAPI-DNA interaction with compound **10a** shows a strong emission at λ_{em} = 465 nm when excited at λ_{exc} = 360 nm (Figure 6). Moreover, Figure 6 also depicts the emission spectra of DAPI bound to CT-DNA in both the absence and presence of the selected compound. When spiro-molecules were added to the DNA in the presence of the DAPI dye, the DNA emission intensity of DAPI decreased.

Moderate quenching behavior was observed in the fluorescence intensity of the DAPI-DNA adduct following the addition of increasing concentrations of SCTz. According to the quenching constant (K_{SV}) values found for the derivatives, this occurred due to greater competition of the molecules for the minor groove when compared to the EB intercalator dye (Table 5).

In general, the Stern-Volmer quenching constants (K_{SV}) of SCTz were calculated and summarized in Table 5. Derivatives containing the CH_3O group compete more strongly with DNA minor grooves, following the increasing general order of (K_{SV}): **EB-DNA** < **DAPI-DNA**. In addition, the high values observed for the bimolecular quenching constant rate (k_q) indicated a static interaction between spiro-derivatives and DNA in all cases (Table 5). The CT-DNA interactive emission spectra of all derivatives are presented in *Supplementary Information* (Figs. S82-S92).

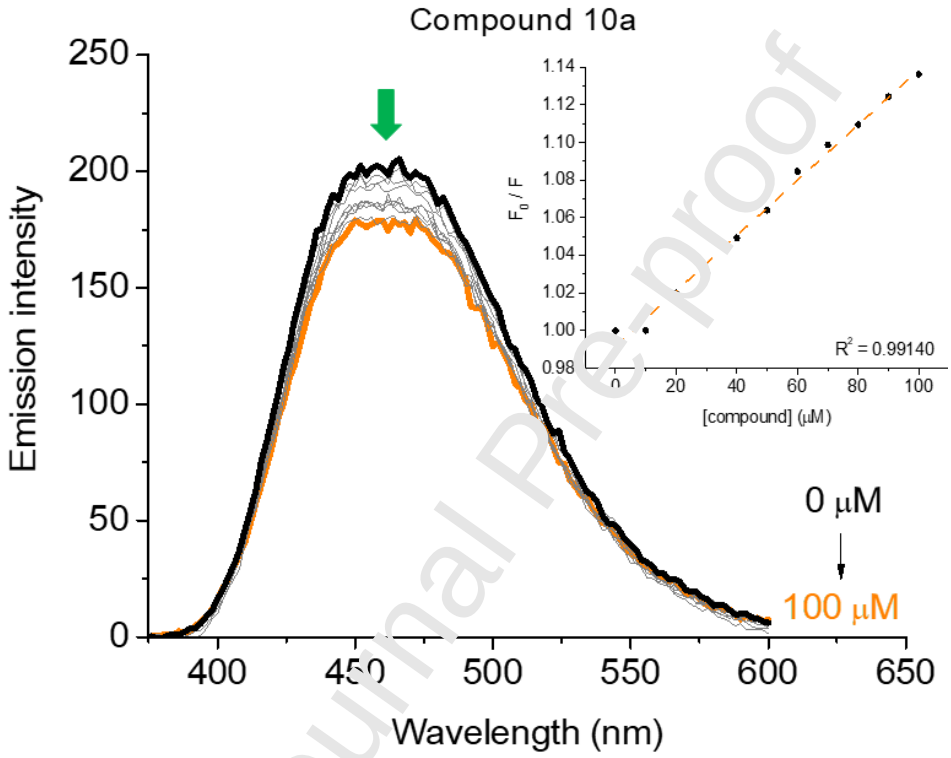

Figure 6. Steady-state emission fluorescence spectra of DAPI-DNA assays in the presence of compound **10a** in a DMSO (2%)/Tris-HCl buffer solution (pH 7.4) at λ_{exc} = 359 nm. The arrow indicates the changes in fluorescence at increasing concentrations of samples. *Insert graph*: plot of F_0/F *versus* [DNA].

Table 5. Competitive dye-DNA values by steady-state fluorescence emission analysis for SCTz.

	EB-DNA emission		
Compound	***Q*%**[a]	**K_{SV} (M^{-1})**[b]	**k_q ($M^{-1}s^{-1}$)**[c]
10a	4.70	5.16×10^2	2.24×10^{10}
10b	5.15	6.09×10^2	2.64×10^{10}
10c	6.90	6.32×10^2	2.74×10^{10}
11a	3.80	4.76×10^2	2.07×10^{10}
11b	6.55	4.20×10^2	1.82×10^{10}
11c	7.25	7.43×10^2	3.23×10^{10}

12a	5.55	6.71×10^2	2.92×10^{10}
12b	4.50	5.65×10^2	2.45×10^{10}
12c	5.60	5.70×10^2	2.48×10^{10}
13a	4.35	4.68×10^2	2.03×10^{10}
13b	5.60	6.01×10^2	2.61×10^{10}
13c	4.20	4.00×10^2	1.74×10^{10}
	DAPI-DNA emission		
Compound	***Q*%[a]**	**K_{SV} (M^{-1})[b]**	**k_q ($M^{-1}s^{-1}$)[d]**
10a	11.20	1.47×10^3	6.68×10^{11}
10b	6.30	0.77×10^3	3.50×10^{11}
10c	12.80	0.75×10^3	3.41×10^{11}
11a	6.15	0.68×10^3	3.09×10^{11}
11b	11.15	1.36×10^3	6.18×10^{11}
11c	5.20	0.72×10^3	3.27×10^{11}
12a	11.05	1.33×10^3	6.04×10^{11}
12b	4.80	0.49×10^3	6.22×10^{11}
12c	12.83	5.65×10^3	2.57×10^{12}
13a	5.90	0.57×10^3	2.59×10^{11}
13b	8.25	0.67×10^3	3.04×10^{11}
13c	7.85	0.82×10^3	3.72×10^{11}

[a]Quenching: $Q(\%) = (\text{Max. initial emission} - \text{Max. final emission}) / (\text{Max. initial emission}) \times 100$;

[b]Stern-Volmer quenching constant by steady-state fluorescence emission;

[c]Bimolecular quenching rate EB-DNA constant by steady-state emission spectra ($\tau_0 = 23$ ns);

[d]Bimolecular quenching rate DAPI-DNA constant by steady-state emission spectra ($\tau_0 = 2.2$ ns).

HSA-binding properties by steady-state fluorescence emission

Steady-state emission fluorescence spectroscopy can be used to monitor damage to human serum albumin (HSA) upon spiro-derivative binding. In principle, these interactions can produce changes in the position or orientation of the tryptophan residue, altering its exposure to solvents and leading to alterations in relative fluorescence properties.[50,51]

The Stern-Volmer quenching (K_{SV}), bimolecular quenching rate (*k*q), and association (K_a) constants were evaluated from the linear plots of emission intensities *versus* spiro-derivative concentration and quenching values (Table 6). The significant Stern-Volmer quenching (10^3 - 10^4 M^{-1} range) and association constant values (10^3 M^{-1} range) obtained for the SCTz suggest there is good interaction between the compounds and HSA proteins.[52]

Higher values of quenching rate constants (*k*q) were observed for spiro-derivatives (10^{11} - 10^{12} M^{-1} s^{-1} range), indicating that steady-state fluorescence quenching probably occurs via static mechanism with the formation of a complex HSA:compound in the ground state (Table 6).[43] Moreover, the number of binding sites (*n*) in all compounds between 0.7 to 1.60 suggests the presence of possible double binding sites for the compounds in the HSA subunits. All HSA fluorescence emission spectra are shown in *Supplementary Information* (Figs. S93-S103).

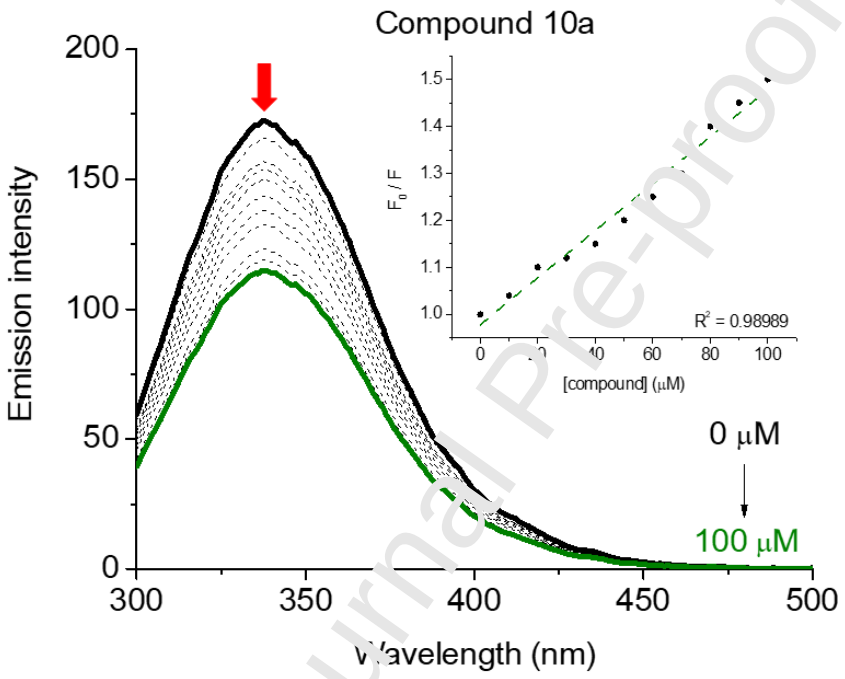

Figure 7. Steady-state emission fluorescence quenching spectra of HSA in the absence and presence of spiro-compound **10a** in a DMSO (2%)/Tris-HCl buffer solution (pH 7.4) at λ_{exc} = 290 nm. The arrow indicates the changes in fluorescence at increasing concentrations of SCTz samples. *Insert graph*: plot of F_0/F *versus* [compound].

Table 6. Stern–Volmer quenching constant (K_{SV}), quenching rate constant (k_q), association constant (K_a), and the number of binding site (*n*) values for the interactions of SCTz with human serum albumin (HSA).

Compound	***Q*(%)[a]**	**K_{SV} (M^{-1})[b]**	**k_q ($M^{-1}s^{-1}$)[c]**	**K_a (M^{-1})[d]**	***n*[e]**
10a	33.40	5.00 x 10^3	8.81 x 10^{11}	3.93 x 10^3	1.06
10b	19.00	2.55 x 10^3	4.50 x 10^{11}	2.65 x 10^3	0.88
10c	33.30	3.65 x 10^3	6.44 x 10^{11}	2.63 x 10^3	0.76
11a	39.50	6.70 x 10^3	1.18 x 10^{12}	4.08 x 10^3	1.07
11b	46.15	8.26 x 10^3	1.45 x 10^{12}	3.30 x 10^3	0.84

11c	41.20	7.34×10^3	1.29×10^{12}	4.07×10^3	1.04
12a	59.80	1.42×10^4	2.50×10^{12}	4.88×10^3	1.19
12b	57.80	1.33×10^4	2.34×10^{12}	6.30×10^3	1.53
12c	57.90	1.24×10^4	2.18×10^{12}	6.33×10^3	1.54
13a	39.40	6.50×10^3	1.14×10^{12}	4.38×10^3	1.13
13b	43.60	7.75×10^3	1.36×10^{12}	4.58×10^3	1.16
13c	43.15	7.72×10^3	1.36×10^{12}	4.62×10^3	1.18

[a]Quenching = $(Int_{initial} - Int_{final}) / Int_{initial} \times 100$; [b]Stern–Volmer quenching constant; [c]Stern–Volmer quenching rate constant (HSA – τ_0 = 5.67 ns); [d]Binding constant; [e]Binding site values.

Molecular docking calculations with DNA and HSA

The computational docking simulation suggested that SCTz**10-13a-c** molecules interact in the minor groove region of the DNA (Figures 3 and S108), which is consistent with the experimental CT-DNA binding assay. In general, all molecules presented similar binding poses, interacting in the groove between dC9, dG10, and dC11 residues from DNA strand A and the dG14, dC15, and dG16 residues from DNA strand B. Van der Waals (vdW) and H-bond are the main interactions (Table S2), with their distances ranging from 3.3 to 4.1 Å and from 1.9 to 2.3 Å, respectively. The OCH_3 group from the **12a-c** derivatives may assist in the interaction with the sugar-phosphate backbone of dC9 and dG10 and, perhaps, may be linked to the strong competition with DNA minor groove. Here, we highlight that the 1,2,3-triazole moiety has an important role as an H-acceptor in the binding of **10-13a-c** molecules with the DNA due to its H-bond with the hydrogen from the amino group of dG10 and dG16 (Figure 8). The involved triazole region in the interaction can be observed in the MEP analysis (Figure 2). Hemamalini[53] and Saini[54] reported that 1,2,3-triazole derivatives interact in the minor groove of DNA and make H-bonds with the nitrogenated base pairs.

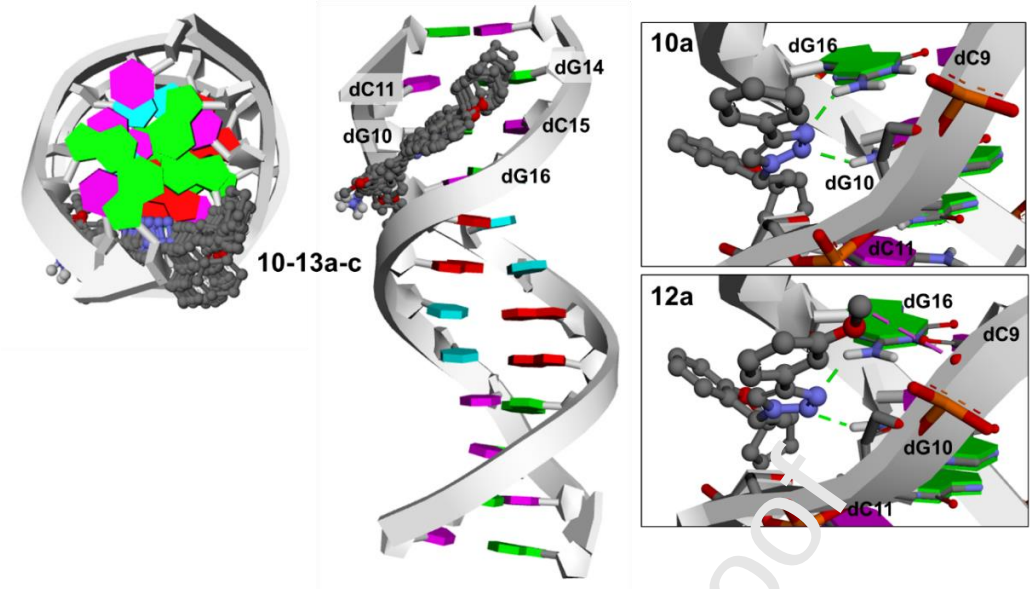

Figure 8. Overview of the best docking pose between DNA and SCTz compounds **10-13a-c**. DNA rings in red, blue, pink, and green indicate deoxyadenosine (dG), deoxythymidine (dT), deoxycytidine (dC), and deoxyguanosine (dG), respectively. dC9, dG10, and dC11 correspond to DNA strand A, while dG14, dC15, and dG16 correspond to DNA strand B. As an example, the **10a** and **12a** H-bonds are highlighted by green-dotted lines. Only the polar hydrogen atoms are shown. More details can be found in *Supporting Information*.

The blind-docking simulations with the HSA protein indicate that SCTz compounds **10a-c**, **11a-c**, **12b**, and **13a-c** interact with HSA subunit IB, while **12a** and **12c** bind in the region between subunits IB and IIA (Figures 9 and S109). SCTz series **10a-c**, **11a-c**, **12b**, and **13a-c** interact mainly with Leu115, Tyr138, Ile142, Tyr161, and Arg186 residues by hydrophobic interactions (π-alkyl, π-π, π-alkyl, and alkyl-alkyl). In addition, the 1,2,3-triazole moiety makes an H-bond with the hydroxyl group of Tyr161 (Table S2). The molecules **12a** and **12c** interact with Lys195, Cys245, and His242 by hydrophobic interactions and with the Arg257 and His242 by H-bond. Notably, the carbon atoms from the side chain of the Lys, Cys, and Arg residues showed hydrophobic interactions. These observations are in accordance with the experimental data. Previous studies have indicated that the interactions of triazole derivatives in the IB (Leu115, Tyr138, and Tyr161) and IIA subunits (His242 and Arg257) may be involved in HSA fluorescence quenching.[55–57] In addition, these regions correspond to the FA1 and FA2 sites where the heme and ibuprofen bind, respectively.[58] The predicted theoretical thermodynamic data (ΔG) indicated that **10-13a-c** present spontaneous interactions with DNA and HSA (Table S2). In general, the aromatic rings and spirocarbocyclic moiety are essential for hydrophobic interactions and the triazole group as a role of H-bond acceptor.

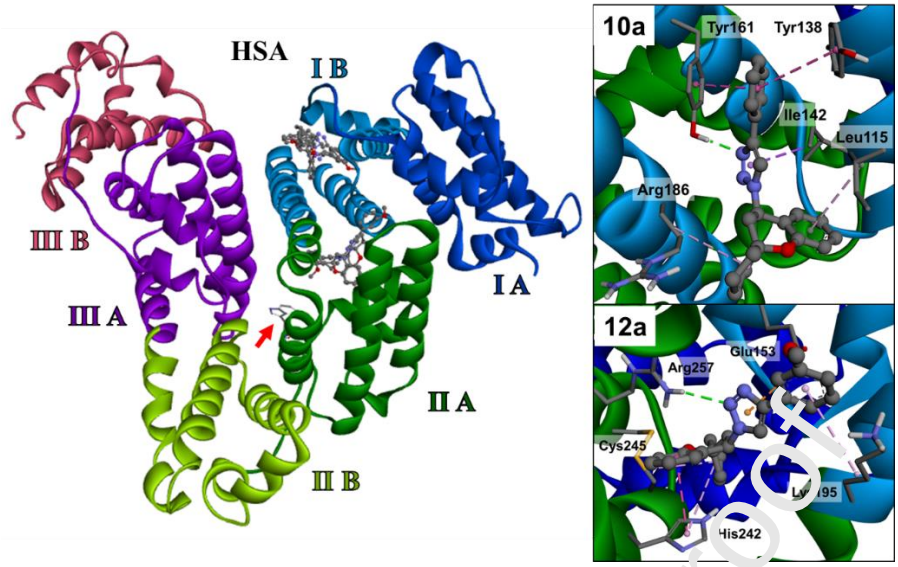

Figure 9. Overview of the best docking pose between HSA and SCTz compounds **10-13a-c**. As an example, **10a** and **12a** interactions are highlighted. The H-bonds, hydrophobic interactions (π-alkyl, π-π, and alkyl-alkyl), and electrostatic interactions (π-anion and π-cation) are shown in green, purple, and orange dotted lines, respectively. Only the polar hydrogen atoms are shown. The Trp214 residue is indicated by the red arrow. HSA domains IA (1–112), IB (113–195), IIA (196–303), IIB (304–383), IIIA (384–500), and IIIB (501–584) are represented by different colors. More details can be found in *Supporting Information.*

Conclusions

In summary, we described a useful and convenient route to prepare novel 1,2,3-triazoles-spirochromanes, namely, 4-(alkyl/aryl)-1-(spiro[chroman-2,1'-cycloalkan]-4-yl)-1*H*-1,2,3-triazoles (SCTz **10-13**) in satisfactory yields. This was easy carried out via Copper-Catalyzed Azide–Alkyne Cycloaddition (CuAAC) reaction involving 4-azidospiro[chroman-2,1'-cycloalkanes] (**5a-c**) and some selected alkynes as precursors. The optimal reaction medium was using copper catalysts ($CuSO_4.5H_2O$/Sodium Ascorbate), THF:H_2O as solvent at room temperature for 24 h. The QTAIM analysis showed intramolecular interactions only in compound **10b**, which is due to the high proximity between the hydrogen atoms rather than an electrostatic potential complementarity. In the case DNA-binding assays by UV-Vis analysis, blue or red-shifts were observed depending on the substituent and all SCTz demonstrated strong binding forces to CT-DNA ($K_b \approx 10^6$ M^{-1}) following the increasing order of K_b values: **12c** < **13c** < **11a** < **10b** < **10a** ≈ **13a** < **13b** < **11c** < **10c** < **12b** < **11b** < **12a**. Besides that, the Stern-Volmer quenching constants (K_{SV}) of SCTz series were calculated and

derivatives showed that the compounds (**12a-c**) compete more strongly with DNA minor grooves, following the increasing general order of (K_{SV}): EB-DNA < DAPI-DNA. The Stern-Volmer and association constant values obtained for the SCTz series imply there is good interaction between the compounds and albumin pocket.

This initial study showed a very accessible synthesis for a new heterocyclic scaffold, which presents interesting photophysical and biointeraction properties that can be contribute to the development of multi– and trans–disciplinary for integrated investigations already in progress.

Experimental

Materials and methods

Unless otherwise indicated, all common reagents and solvents were used as obtained from commercial suppliers, without further purification. The melting points were determined using glass capillary tubes in an Electrothermal MEL-TEMP 3.0 apparatus, and are uncorrected. ^{1}H and ^{13}C NMR spectra were acquired either in a Bruker DPX 200 (^{1}H at 200 MHz), Bruker AVANCE NANOBAY V3-I-400 MHz (^{1}H at 400 MHz and ^{13}C at 100 MHz) or Bruker Avance III (^{1}H at 600 MHz and ^{13}C at 150 MHz) with 5 mm sample tubes, 298 K, digital resolution of 0.01 ppm, in $CDCl_3$, and using TMS as an internal reference. The ^{19}F NMR spectra were acquired on a Bruker Avance III DPX 600, at 564.68 MHz, with 5 mm sample tubes at 298 K, digital resolution of 0.01 ppm, in $CDCl_3$, and using $CFCl_3$ (d 0.0 ppm) as the external reference. The 2D spectra were acquired on a Bruker Avance III DPX 600 (^{1}H at 600 MHz and ^{13}C at 150 MHz), with 5 mm sample tubes, solutions at 298 K, digital resolution of 0.01 ppm, in $CDCl_3$, and using TMS as internal reference. Mass spectra were performed in a HP 5973 MSD spectrometer connected to a HP 6890 GC spectrometer. The GC spectrometer was equipped with a split-splitless injector, auto sampler, cross-linked HP-5 capillary column (30 m, 0.32 mm internal diameter), and helium was used as the carrier gas.

Single Crystal X-ray Diffraction (SC-XRD)

Suitable single crystals were obtained by slow evaporation of EtOH at 25 °C. Diffraction measurements were performed using a Bruker D8 Venture diffractometer equipped with a Photon 100 CMOS detector, using Mo Kα radiation (λ = 0.71073 Å), for compounds **10b**, **11b**, **12b-c**, and **13c**. Absorption corrections were performed using multi-scan methods. The structures were solved using SHELXS[59] or olex2.solve,[60] and refinements were carried out using SHELXL 2018/3[61] with the aid of the software Olex2 1.3.[62] Anisotropic displacement parameters for non-hydrogen atoms were applied. The molecular diagrams were generated using the software Mercury.[63] Crystal structure parameters of compound **10b**, **11b**, **12b-c**, and **13c** are listed in Table S1 in *Supporting Information*. Crystallographic information file (CIF) for compounds **10b**, **11b**, **12b, 12c**, and **13c** were deposited at the Cambridge Crystallographic Data Centre (CCDC) under identification number 1996495, 2013986, 1996330, 1996331, and 1996496, respectively.

Quantum Mechanical Calculations

The performed calculations were performed with geometries obtained from SC-XRD. Density functional theory (DFT) calculations were performed using the Gaussian 09 software package[64] with ωB97x-D/cc-pVDZ theory level. The counterpoise method of Boys and Bernardi was employed to minimize the basis set superposition error (BSSE).[65] QTAIM analyses were performed with the aid of the AIMALL software package.[66] The wavefunctions used in the QTAIM and MEP analyses were generated at the ωB97x-D/cc-pVDZ level of theory. MEP maps were built on the electron density 0.01 a.u. isosurface with GaussView.[67]

Absorption UV-Vis analysis

UV-Vis absorption spectra were recorded using Shimadzu UV2600 spectrophotometer (data interval, 1.0 nm) using dimethyl sulfoxide (DMSO) as solvent.

CT-DNA interactions by absorption and fluorescence emission

For DNA-binding assays, compound interactions with calf-thymus DNA (CT-DNA) were performed by UV-vis absorption measurements at room temperature in Tris-HCl buffer at pH 7.4 using DMSO stock solution of derivatives (~10^{-4} M range) at the range of 250 to 600 nm. The DNA pair base concentrations of low molecular weight DNA from calf thymus (ct-DNA) was determined by absorption spectroscopy using the molar extinction coefficients 6,600 $M^{-1}cm^{-1}$ (per base pair) at λ_{max} = 260 nm, respectively. Derivative solutions in DMSO with Tris-HCl buffer were titrated with increasing concentrations of DNA (ranging from 0-100 μM). The intrinsic binding constants (K_b) of derivatives were calculated according to the decay of the absorption bands of compounds using the following equation (1) through a plot of [DNA]/($\varepsilon_a - \varepsilon_f$) *versus* [DNA]:

$$[DNA]/(\varepsilon_a - \varepsilon_f) = [DNA]/(\varepsilon_b - \varepsilon_f) + 1/K_b(\varepsilon_b - \varepsilon_f) \quad (1)$$

where [DNA] is the concentration of DNA in the base pairs, ε_a is the extinction coefficient (A_{obs}/[compound]), and ε_b and ε_f are the extinction coefficients of free and fully bound forms, respectively. In plots of [DNA]/($\varepsilon_a - \varepsilon_f$) *versus* [DNA], K_b is given by the ratio of the slope for the intercept ion.

The standard Gibbs free-energy (ΔG^o) of compound-DNA adduct was calculated from the values of binding constant (K_b) using the following equation (2):

$$\Delta G^o = -RT \ln K_b \quad (2)$$

where R and T are the gas constant (1.987 kcal K^{-1} mol^{-1}) and temperature (298 K), respectively.

Steady-state emission fluorescence analyses of SCTz series were measured with a Varian Cary 50 fluorescence spectrophotometer (Exc./Em; slit 2.0 mm/2.0 mm) and corrected according to the manufacturer's instructions. In competition dye-DNA assays, steady-state emission fluorescence analysis was recorded and derivatives dissolved in DMSO solutions. Competitive studies were performed through the gradual addition of the stock solution of the spiro-derivatives to the quartz cuvette (1.0 cm path length) containing ethidium bromide (EB, 2.0 x 10^{-7} M) or 4′,6-diamidino-2-phenylindole (DAPI, 2.0 x 10^{-7} M) and DNA (2.0 x 10^{-5} M) in a Tris-HCl pH 7.4 buffer solution. The

concentration of derivatives ranged from 0 to 100 μM. Samples were excited at λ_{exc} = 510 nm (for EB dye) and λ_{exc} = 359 nm (for DAPI dye). Emission spectra were recorded at the range of 350-850 nm, 3.0 min after each addition of the complex solution in order to allow incubation to occur. The fluorescence quenching Stern-Volmer constants (K_{SV}) of compounds were calculated according to the decay of the emission bands of dye-DNA using the following Stern-Volmer equation (3) through a plot of F_0/F *versus* [DNA],

$$F_0/F = 1 + k_q\tau_0[Q] = 1 + K_{SV}[Q] \qquad (3)$$

where F and F_0 are the fluorescence intensities in the presence and absence of a quencher, respectively. K_{SV}, k_q, τ_0 and [Q] denote Stern–Volmer quenching constant, quenching rate constant, lifetime of EB-DNA adducts (τ_0 = 23.0 ns),[68] lifetime of DAPI-DNA adducts (τ_0 = 2.20 ns),[69] and quencher concentration, respectively. According to equation (3), the Stern–Volmer constants (K_{SV}) were calculated from the slope and k_q is equal K_{SV}/τ_0.

HSA-binding properties by steady-state emission fluorescence

For emission HSA experiments, SCTz interactions with human serum albumin (HSA) were performed by steady-state emission fluorescence measurements at room temperature in Tris-HCl buffer at pH 7.4 using DMSO stock solution of derivatives (~10^{-4} M range) at 300 to 500 nm range. It is well known that quenching occurs through the static or dynamic quenching process, both of which can result in a linear Stern–Volmer plot. To analyze the data from the quenching assays, we used the same Stern–Volmer equation (3) above, where F and F_0 are the fluorescence intensities in the presence and absence of a quencher, respectively. K_{SV}, k_q, τ_0 and [Q] denote Stern–Volmer constant, quenching rate constant, the original lifetime of HSA (5.67 ns),[70] and the concentration of quencher, respectively. According to Equation (3), the Stern–Volmer constants (K_{SV}) were calculated from the slope and k_q is equal K_{SV}/τ_0. It is generally accepted that the maximum Stern–Volmer constant allowed for the dynamic quenching of biomolecules is 1.0 x 10^2 M^{-1}. Therefore, to conclude that the quenching is not a dynamic but static process occurring in the HSA-compound complex, Scatchard equation (4) predicted the K_a (association constant) and *n* (binding site):

$$\log (F_0 - F)/F = \log K_a + n \log [Q] \qquad (4)$$

where F_0 and F represent fluorescence intensities in the absence and presence of chalcogen derivatives, respectively, and [Q] the quencher concentration. According to equation (3), the association constants (K_a) were calculated from the interception and the number of binding sites (*n*) for the slope, respectively.

Molecular Docking

Molecular docking is a computational method that predicts the binding-conformation of ligands when interacting with a target. For this purpose, the AutoDock Vina 1.1.1 program was used.[71] The crystallographic structures of DNA and HSA were obtained from the Protein Data Bank (http://www.rcsb.org/pdb/) with the codes 1BNA[72] and 3B9L,[73] respectively. The Chimera 1.8 software[74] was used to remove water, ions, and other molecules and add hydrogen atoms to the DNA and HSA. The compounds **10-13a-c** were built in the software Avogadro 1.1.1,[75] followed by semi-empirical PM6 geometry optimization[76] using the software MOPAC2016[77] (the isomers R were considered as a representative model). The optimized structures of SCTz **10b**, **11b**, **12c**, and **13c** were compared with their crystallography data and the root-mean-square deviation (RMSD) values (0.184, 0.109, 0.228, and 0.125 Å, respectively) indicated that the PM6 geometry optimization could reproduce the experimental data. The ligands and macromolecules in the *pdbqt* format were generated by AutoDockTools, where the ligands were considered flexible (with PM6 charges) and the DNA/HSA rigid (with Gasteiger charges).[78] The blind docking was used for both targets using the grid box size of 50 x 50 x 50 Å (coordinates: x = 14.8, y = 21.0, z = 12.3) and 90 x 50 x 90 Å (coordinates: x = 29.3, y = 0.4, z = 19.2) for DNA and HSA, respectively, with 1.0 Å of grid spacing. As a model of interactions, the conformer of the lowest binding free energy was selected. The results from the docking simulations were analyzed using the Accelrys Discovery Studio 3.5 software.[79]

Synthesis

*General procedure for the synthesis of 4-(alkyl/aryl)-1-(spiro[chroman-2,1'-cycloalkan]-4-yl)-1H-1,2,3-triazoles (SCTz **10a-c**, **11a-c**, **12a-c**, **13a-c**)*

To a 25 mL flask containing a THF/H_2O solution 1:1 v/v (5 mL) used as the reaction solvent at room temperature and under magnetic stirring, the 4-azidospirochromanes (**5a-c**) (1mmol) and terminal alkynes (**6-9**) (1.1 mmol) were added after sodium ascorbate (20 mol%) and copper sulfate pentahydrate (10 mol%). After the reaction completation (24 h), the mixture was extracted into ethyl acetate (2 x 10mL) and distilled water (5mL). The organic phase was dried over sodium sulfate and filtered. The solvent was then removed in the rotary evaporator under reduced pressure and the SCTz compounds purified by column chromatography employing a 10% solution of ethyl acetate in hexane (**10a-c**), (**12a-c**), (**13a-c**), and 30% solution of ethyl acetate in hexane (**11a-c**) as eluent.

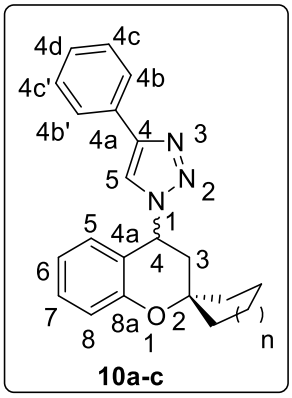

10a-c

4-Phenyl-1-(spiro[chroman-2,1'-cyclopentan]-4-yl)-1H-1,2,3-triazole **10a**

White solid, yield 70%, m.p. 175–180 °C. ^{1}H NMR (400 MHz, $CDCl_3$) **Triazole:** δ 7.84 (d, *J* = 7.5 Hz, 2H, H-4c/H-4c'), 7.67 (s, 1H, H-5), 7.43 (t, *J* = 7.5 Hz, 2H, H-4b/H-4b'), 7.35 (t, *J* = 7.5 Hz, 1H, H-4d). **Chromane:** δ 7.30-7.22 (m, 1H, H-7), 6.95-6.88 (m, 1H, H-5), 6.90-6.81 (m, 1H, H-6/H-8), 6.13 (dd, $^1J_{H\text{-}H}$ = 10.5 Hz $^2J_{H\text{-}H}$ = 5.5 Hz, 1H, H-4), 2.64 (dd, $^1J_{H\text{-}H}$ = 13 Hz $^2J_{H\text{-}H}$ = 10.5 Hz, 1H, H-3a), 2.49 (dd, $^1J_{H\text{-}H}$ = 13.0 Hz $^2J_{H\text{-}H}$ = 5.5 Hz, 1H, H-3a'), 2.08-1.63 (m, 8H, 4CH_2). ^{13}C NMR (100 MHz, $CDCl_3$) **Triazole:** δ 148.1 (C-4a), 130.5 (C-4), 128.8 (C-4c/C-4c'), 128.2 (C-4d), 125.6 (C-4b/C-4b'), 117.9 (C-5). **Chromane:** δ 154.0 (C-8a), 130.1 (C-7), 127.8 (C-8), 120.8 (C-6), 119.1 (C-4a), 118.1 (C-5), 86.2 (C-2), 55.4 (C-4), 39.1 (C-3), 39.0 (CH_2), 36.3 (CH_2), 23.8 (CH_2), 23.7 (CH_2). HRMS Calcd. for $C_{21}H_{21}N_3O$: 332.1763. Found: 332.1757.

4-Phenyl-1-(spiro[chroman-2,1'-cyclohexan]-4-yl)-1H-1,2,3-triazole **10b**

White solid, yield 70%, m.p. 164–166 °C. ^{1}H NMR (400 MHz, $CDCl_3$) **Triazole:** δ 7.83 (d, *J* = 7 Hz, 2H, H-4c/H-4c'), 7.66 (s, 1H, H-5), 7.46-7.37 (m, 2H, H-4b/H-4b'), 7.33

(t, *J* = 7.5 Hz, 1H, H-4d). **Chromane:** δ 7.31-7.21 (m, 1H, H-7), 7.01-6.94 (m, 1H, H-5), 6.90-6.80 (m, 2H, H-6/H-8), 6.14 (dd, $^{1}J_{H\text{-}H}$ = 11.5 Hz $^{2}J_{H\text{-}H}$ = 6.5 Hz, 1H, H-4), 2.52 (dd, $^{1}J_{H\text{-}H}$ = 13 Hz $^{2}J_{H\text{-}H}$ = 6.5 Hz, 1H, H-3a), 2.29 (dd, $^{1}J_{H\text{-}H}$ = 13 Hz $^{2}J_{H\text{-}H}$ = 11.5 Hz, 1H, H-3a'), 1.99-1.37 (m, 10H, 5CH_2). ^{13}C NMR (100 MHz, $CDCl_3$) **Triazole:** δ 148.3 (C-4a), 130.6 (C-4), 128.8 (C-4c/C-4c'), 128.1 (C-4d), 125.7 (C-4b/C-4b'), 117.8 (C-5). **Chromane:** δ 153.6 (C-8a), 130.1 (C-7), 127.5 (C-8), 120.7 (C-6), 119.2 (C-4a), 118.0 (C-5), 76.1 (C-2), 54.2 (C-4), 40.1 (C-3), 37.8 (CH_2), 32.3 (CH_2), 25.5 (CH_2), 21.5 (2CH_2). GC-MS (EI, 70 (eV): *m/z* 345 (M^+, 100), 250 (26), 201 (34). HRMS Calcd. for $C_{22}H_{23}N_3O$: 346,1921. Found: 346.1914.

.

4-Phenyl-1-(spiro[chroman-2,1'-cycloheptan]-4-yl)-1H-1,2,3-triazole **10c**

White solid, yield 95%, m.p. 163–165 °C. ^{1}H NMR (400 MHz, $CDCl_3$) **Triazole:** δ 7.82-7.78(m, 2H, H-4c/H-4c'), 7.64 (s, 1H, H-5), 7.43-7.40 (m, 2H, H-4b/H-4b'), 7.34-7.29 (m, 1H, H-4d). **Chromane:** δ 7.25-7.19 (m, 1H, H-7), 6.93-6.88 (m, 1H, H-5), 6.85-6.79 (m, 1H, H-6), 6.78-6.74 (m, 1H, H-8), 6.07 (dd, $^{1}J_{H\text{-}H}$ = 12 Hz $^{2}J_{H\text{-}H}$ = 6 Hz, 1H, H-4), 2.57 (dd, $^{1}J_{H\text{-}H}$ = 13, $^{2}J_{H\text{-}H}$ = 6, 1H, H-3a), 2.22 (dd, $^{1}J_{H\text{-}H}$ = 13, $^{2}J_{H\text{-}H}$ = 12, 1H, H-3a'), 2.08-1.39 (m, 12H, 6CH_2). ^{13}C NMR (100 MHz, $CDCl_3$) **Triazole:** δ 148.3 (C-4a), 130.5 (C-4), 128.8 (C-4c/C-4c'), 128.2 (C-4d), 125.6 (C-4b/C-4b'), 117.8 (C-5). **Chromane:** δ 153.6 (C-8a), 130.1 (C-7), 127.4 (C-8), 120.7 (C-6), 119.3 (C-4a), 118.1 (C-5), 80.5 (C-2), 54.4 (C-4), 41.5 (C-3), 41.1 (CH_2), 35.3 (CH_2), 29.8 (CH_2), 29.7 (CH_2), 22.0 (CH_2), 21.8 (CH_2). HRMS Calcd. for $C_{23}H_{25}N_3O$: 360.2076. Found: 360.2070.

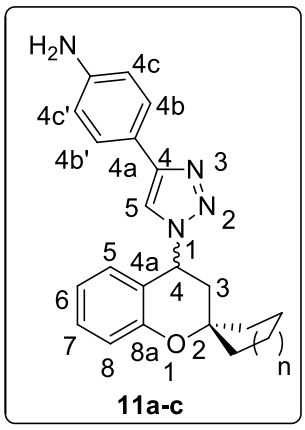

11a-c

4-(1-(Spiro[chroman-2,1'-cyclopentan]-4-yl)-1H-1,2,3-triazol-4-yl) aniline **11a**

Brown solid, yield 47%, m.p. 224-225 °C. ^{1}H NMR (400 MHz, $CDCl_3$) **Triazole:** δ 7.63-7.59 (m, 2H, H-4b/H-4b'), 7.50 (s, 1H, H-5), 6.74-6.70 (m, 2H, H-4c/H-4c'), 3.75 (s, 2H, NH_2). **Chromane:** δ 7.29-7.19 (m, 1H, H-7), 6.91-6.87 (m, 1H, H-5), 6.86-6.81 (m, 2H, H-6/H-8), 6.09 (dd, $^{1}J_{H-H}$ = 11 Hz $^{2}J_{H-H}$ = 6.5 Hz, 1H, H-4), 2.61 (dd, $^{1}J_{H-H}$ = 13 Hz $^{2}J_{H-H}$ = 11 Hz, 1H, H-3a), 2.44 (dd, $^{1}J_{H-H}$ = 13 Hz $^{2}J_{H-H}$ = 6 Hz, 1H, H-3a'), 1.96-1.26 (m, 8H, $4CH_2$). ^{13}C NMR (100 MHz, $CDCl_3$) **Triazole:** δ 148.5 (C-4a), 146.5 (C-4d), 126.9 (C-4b/C-4b'), 120.7 (C-4), 116.5 (C-5), 115.2 (C-4c/C-4c'). **Chromane:** δ 153.9 (C-8a), 130.0 (C-7), 127.8 (C-8), 121.0 (C-4a), 119.3 (C-6), 118.0 (C-5), 86.2 (C-2), 55.3 (C-4), 39.0 (C-3), 36,2 ($2CH_2$), 23.9 (CH_2), 23.7 (CH_2). GC-MS (EI, 70 (eV): *m/z* (%) 361 (M^+, 100), 304 (31), 77 (33). HRMS: Calcd. $C_{21}H_{22}N_4O$: 347.1866. Exp: 347.1870.

4-(1-(Spiro[chroman-2,1'-cyclohexan]-4-yl)-1H-1,2,3-triazol-4-yl) aniline **11b**

Brown solid, yield 54%, m.p. 220-221 °C. ^{1}H NMR (400 MHz, $CDCl_3$) **Triazole:** δ 7.62-7.57 (m, 2H, H-4b/H-4b'), 7.51 (s, 1H, H-5), 6.73-6.68 (m, 2H, H-4c/H-4c'), 3.81 (s, 2H, NH_2). **Chromane:** δ 7.24-7.21 (m, 1H, H-7), 6.96-6.91 (m, 1H, H-5), 6.84-6.81 (m, 1H, H-6), 6.79-6.77 (m, 1H, H-8), 6.09 (dd, $^{1}J_{H-H}$ = 11.5 Hz $^{2}J_{H-H}$ = 6.5 Hz, 1H, H-4), 2.48 (dd, $^{1}J_{H-H}$ = 13.5 Hz $^{2}J_{H-H}$ = 6.5 Hz, 1H, H-3a), 2.25 (dd, $^{1}J_{H-H}$ = 13 Hz $^{2}J_{H-H}$ = 11,5 Hz, 1H, H-3a'), 1.96-1.26 (m, 10H, $5CH_2$). ^{13}C NMR (100 MHz, $CDCl_3$) **Triazole:** δ 148.3 (C-4a), 146.3 (C-4d), 126.9 (C-4b/C-4b'), 120.7 (C-4), 116.4 (C-5), 115.2 (C-4c/C-4c'). **Chromane:** δ 153.6 (C-8a), 130.0 (C-7), 127.4 (C-8), 121.0 (C-4a), 119.5 (C-6), 118.0 (C-5), 82.5 (C-2), 54.3 (C-4), 40.1 (C-3), 37.9 (CH_2), 32.2 (CH_2), 29.6 (CH_2), 25.5 (CH_2), 21.5 (CH_2). LC-MS (EI, 70 (eV): *m/z* (%) 361 (M+, 100), 304 (31), 77 (33). HRMS: Calcd. $C_{22}H_{24}N_4O$: 361.2023. Exp: 361.2025.

4-(1-(Spiro[chroman-2,1'-cycloheptan]-4-yl)-1H-1,2,3-triazol-4-yl) aniline **11c**

Brown solid, yield 50%, m.p. 190-191°C. ^{1}H NMR (400 MHz, $CDCl_3$) **Triazole:** δ 7.63-7.59 (m, 2H, H-4b/H-4b'), 7.51 (s, 1H, H-5), 6.73-6.71 (m, 2H, H-4c/H-4c'), 3.58 (s, 2H, NH_2). **Chromane:** δ 7.26-7.21 (m, 1H, H-7), 6.93-6.91 (m, 1H, H-5), 6.86-6.77 (m, 2H, H-6/H-8), 6.06 (dd, $^{1}J_{H-H}$ = 11.5 Hz $^{2}J_{H-H}$ = 6.0 Hz, 1H, H-4), 2.57 (dd, $^{1}J_{H-H}$ = 13.0 Hz $^{2}J_{H-H}$ = 6.0 Hz, 1H, H-3a), 2.27-2.19 (m, 1H, H-3a'), 1.87-1.29 (m, 12H, $6CH_2$). RMN ^{13}C (100MHz, $CDCl_3$) **Triazole:** δ 148.6 (C-4a), 146.5 (C-4d), 126.9 (C-

4b/C-4b'), 120.6 (C-4), 116.4 (C-5), 115.2 (C-4c/C-4c'). **Chromane:** δ 153.6 (C-8a), 130.0 (C-7), 127.6 (C-8), 120.7 (C-6), 119.4 (C-4a), 117.9 (C-5), 76.1 (C-2), 54.0 (C-4), 41.5 (C-3), 41.0 (CH_2), 35.3 (CH_2), 29.7 (CH_2), 29.6 (CH_2), 22.0 (CH_2), 21.8 (CH_2). LC-MS (EI, 70 eV): *m/z* (%) 375 (M+, 100), 215, 161, 102. HRMS: Calcd. $C_{23}H_{26}N_4O$: 375.2179. Exp: 375.2182.

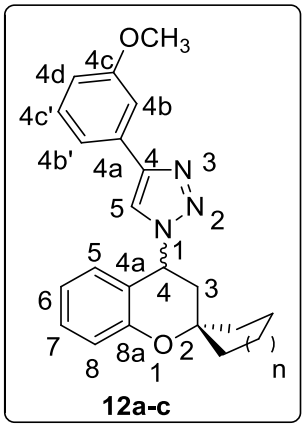

12a-c

4-(3-Methoxyphenyl)-1-(spiro[chroman-2,1'-cyclopentan]-4-yl)-1H-1,2,3-triazole **12a**

White solid, yield 60%, m.p. 145-146 °C. ^{1}H NMR (400 MHz, $CDCl_3$) **Triazole:** δ 7.67 (s, 1H, H-5), 7.49-7.43 (m, 1H, H-4c'), 7.36-7.29 (m, 2H, H-4b/H-4b'), 6.97 (dd, $^1J_{H-H}$ = 8 Hz, $^2J_{H-H}$ = 1 Hz, 1H, H-4d) 3.88 (s, 3H, CH_3). **Chromane:** δ 7.28-7.23 (m, 1H, H-7), 6.93-6.85 (m, 2H, H-5/H-6), 6.84-6.79 (m, 1H, H-8), 6.13 (dd, $^1J_{H-H}$ = 11.5 Hz $^2J_{H-H}$ = 6.5 Hz, 1H, H-4), 2.54-2.43 (m, 1H, H-3a), 2.28 (dd, $^1J_{H-H}$ = 13 Hz $^2J_{H-H}$ = 11,5 Hz, 1H, H-3a'), 2.14-1.34 (m, 8H, 4CH_2). RMN ^{13}C (100MHz, $CDCl_3$) **Triazole:** δ 160.0 (C-4c), 148.3 (C-4a), 131.7 (C-4), 130.1 (C-4c'), 118.0 (C-5), 114.5 (C-4d), 110.6 (C-4b/C-4b'), 54.2 (CH_3). **Chromane:** δ 153.6 (C-8a), 129.8 (C-7), 127.8 (C-8), 120.7 (C-6), 119.2 (C-4a), 118.1 (C-5), 76.1 (C-2), 55.3 (C-4), 40.1 (C-3), 37.8 (CH_2), 32.2 (CH_2), 25.5 (CH_2), 21.5 (CH_2). LC-MS (EI, 70 eV): *m/z* (%) 362 (M+, 100), 176, 89. HRMS: Calcd. $C_{23}H_{23}N_3O_2$: 362.1863. Exp: 362.1865.

4-(3-Methoxyphenyl)-1-(spiro[chroman-2,1'-cyclohexan]-4-yl)-1H-1,2,3-triazole **12b**

White solid, yield 70%, m.p. 167-168°C. ^{1}H NMR (400 MHz, $CDCl_3$) **Triazole:** δ 7.66 (s, 1H, H-5), 7.49-7.39 (m, 1H, H-4c'), 7.34-7.26 (m, 2H, H-4b/H-4b'), 6.90-6.84 (m, 1H, H-4d) 3.88 (s, 3H, CH_3). **Chromane:** δ 7.26-7.21 (m, 1H, H-7), 6.97-6.92 (m, 1H, H-5), 6.85-6.80 (m, 1H, H-6), 6.80-6.75 (m, 1H, H-8), 6.13 (dd, $^1J_{H-H}$ = 11.5 Hz $^2J_{H-H}$ = 6.5 Hz, 1H, H-4), 2.52 (dd, $^1J_{H-H}$ = 13 Hz, $^2J_{H-H}$ = 6.5 Hz, 1H, H-3a), 2.27 (dd, $^1J_{H-H}$ =

13 Hz $^{2}J_{H\text{-}H}$ = 11.5 Hz, 1H, H-3a'), 1.99-1.26 (m, 10H, 5CH_2). RMN ^{13}C (100MHz, $CDCl_3$) **Triazole:** δ 160.0 (C-4c), 148.3 (C-4a), 131.8 (C-4), 129.8 (C-4c'), 118.0 (C-5), 114.5 (C-4d), 110.6 (C-4b/C-4b'), 54.2 (CH_3). **Chromane:** δ 153.6 (C-8a), 130.1 (C-7), 127.5 (C-8), 120.8 (C-6), 119.2 (C-4a), 118.1 (C-5), 76.1 (C-2), 55.3 (C-4), 40.2 (C-3), 37.8 (CH_2), 32.3 (CH_2), 25.5 (CH_2), 21.5 (CH_2) 21.4 (CH_2). LC-MS (EI, 70 eV): *m/z* (%) 376 (M+, 100), 199, 89. HRMS: Calcd. $C_{23}H_{25}N_3O_2$: 376.2028. Exp: 376.2020.

4-(3-Methoxyphenyl)-1-(spiro[chroman-2,1'-cycloheptan]-4-yl)-1H-1,2,3-triazole **12c**

White solid, yield 85%, m.p. 129-130°C. ^{1}H NMR (400 MHz, $CDCl_3$) **Triazole:** δ 7.66 (s, 1H, H-5), 7.49-7.43 (m, 1H, H-4c'), 7.36-7.29 (m, 2H, H-4b/H-4b'), 6.93-6.85 (m, 1H, H-4d) 3.88 (s, 3H, CH_3). **Chromane:** δ 7.30-7.20 (m, 1H, H-7), 6.97-6.90 (m, 1H, H-5), 6.87-6.83 (m, 1H, H-6), 6.80-6.78 (m, 1H, H-8), 6.09 (dd, $^{1}J_{H\text{-}H}$ = 11.5 Hz $^{2}J_{H\text{-}H}$ = 6.5 Hz, 1H, H-4), 2.60 (dd, $^{1}J_{H\text{-}H}$ = 13 Hz, $^{2}J_{H\text{-}H}$ = 6.5 Hz, 1H, H-3a), 2.25 (dd, $^{1}J_{H\text{-}H}$ = 13 Hz $^{2}J_{H\text{-}H}$ = 11.5 Hz, 1H, H-3a'), 1.90-1.25 (m, 12H, 6CH_2). RMN ^{13}C (100MHz, $CDCl_3$) **Triazole:** δ 160.0 (C-4c), 148.3 (C-4a), 131.8 (C-4), 129.8 (C-4c'), 118.1 (C-5), 114.5 (C-4d), 110.6 (C-4b/C-4b'), 54.4 (CH_3). **Chromane:** δ 153.7 (C-8a), 130.1 (C-7), 127.4 (C-8), 120.7 (C-6), 119.3 (C-4a), 118.1 (C-5), 80.5 (C-2), 55.3 (C-4), 41.5 (C-3), 41.1(CH_2), 35.3 (CH_2), 29.7 (CH_2), 29.6 (CH_2), 22.0 (CH_2) 21.8 (CH_2). GC-MS (EI, 70 eV): *m/z* (%) 389 (50), 280 (48), 215 (45), 157 (M^+, 100). HRMS: Calcd.$C_{24}H_{27}N_3O_2$: 390.2176. Exp: 390.2179.

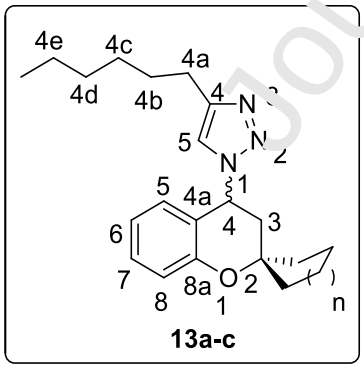

13a-c

4-(4-Hexylphenyl)-1-(spiro[chroman-2,1'-cyclopentan]-4-yl)-1H-1,2,3-triazole **13a**

White solid, yield 90%, m.p. 94-95°C. ^{1}H NMR (400 MHz, $CDCl_3$) **Triazole:** δ 7.15 (s, 1H, H-5), 2.73-2.69 (m, 2H, H-4a), 0.89-0.85 (m, 3H, CH_3) **Chromane:** δ 7.25-7.20 (m, 1H, H-7), 6.91-6.80 (m, 2H, H-6/H-5), 6.79-6.71 (m, 1H, H-8), 6.04 (dd, $^{1}J_{H\text{-}H}$ = 11 Hz $^{2}J_{H\text{-}H}$ = 6 Hz, 1H, H-4), 2.55 (dd, $^{1}J_{H\text{-}H}$ = 13 Hz $^{2}J_{H\text{-}H}$ = 6.5 Hz, 1H, H-3a), 2.40 (dd, $^{1}J_{H\text{-}}$

$_H$ = 13 Hz $^2J_{H-H}$ = 6 Hz, 1H, H-3a'), 1.94-1.24 (m, 18H, 9CH_2). RMN ^{13}C (100 MHz, $CDCl_3$) **Triazole:** δ 153.9 (C-4), 120.6 (C-5), 31.5 (C-4d), 29.3 (C-4c), 28.8 (C-4b), 25.8 (C-4a), 22.5 (C-4e) 14.0 (CH_3). **Chromane:** δ 148.9 (C-8a), 129.9 (C-7), 127.7 (C-5), 119.4 (C-4a), 118.8 (C-6), 118.0 (C-8), 86.2 (C-2), 55.1 (C-4), 39.0 (CH_2), 36.2 (C-3), 23.9 (CH_2), 23.7 (CH_2). GC-MS (EI, 70 eV): *m/z* (%) 339 (16), 230 (8), 187 (M^+, 100), 157 (47). HRMS: Calcd. $C_{21}H_{29}N_3O$: 340.2383. Exp: 340.2387.

4-(4-Hexylphenyl)-1-(spiro[chroman-2,1'-cyclohexan]-4-yl)-1H-1,2,3-triazole **13b**

White solid, yield 60%, m.p. 84-85°C. ^{1}H NMR (400 MHz, $CDCl_3$) **Triazole:** δ 7.15 (s, 1H, H-5), 2.71-2.68 (m, 2H, H-4a), 0.89-0.85 (m, 3H, CH_3). **Chromane:** δ 7.24-7.19 (m, 1H, H-7), 6.91 (d, *J*= 8 Hz, 1H, H-5), 6.84-6.79 (m, 1H, H-6), 6.70 (d, *J*= 7,5 Hz, 1H, H-8), 6.03 (dd, $^1J_{H-H}$ = 12 Hz $^2J_{H-H}$ = 6.5 Hz, 1H, H-4), 2.43 (dd, $^1J_{H-H}$ = 13 Hz $^2J_{H-H}$ = 6.5 Hz, 1H, H-3a), 2.22-2.14 (m, 1H, H-3a'), 1.94-1.24 (m, 18H, 9CH_2). RMN ^{13}C (100 MHz, $CDCl_3$) **Triazole:** δ 149.1 (C-4), 118.7 (C-5), 37.8 (C-4d), 29.3 (C-4c), 28.9 (C-4b), 25.8 (C-4a), 22.5 (C-4e), 14.0 (CH_3). **Chromane:** δ 153.4 (C-8a), 129.9 (C-7), 127.4 (C-8), 120.6 (C-6), 119.5 (C-4a), 117.8 (C-5), 76.1 (C-2), 53.8 (C-4), 40.3 (C-3), 32.3 (CH_2), 31.5 (CH_2), 25.5 (CH_2), 21.4 (CH_2). GC-MS (EI, 70 eV): *m/z* (%) 353 (36), 230 (10), 201 (M^+, 100), 157 (50). HRMS Calcd. for $C_{22}H_{31}N_3O_2$: 354.2543. Found: 354.2540.

4-(4-Hexylphenyl)-1-(spiro[chroman-2,1'-cycloheptan]-4-yl)-1H-1,2,3-triazole **13c**

White solid, yield 60%, m.p. 84-85°C. ^{1}H NMR (400 MHz, $CDCl_3$) **Triazole:** δ 7.15 (s, 1H, H-5), 2.74-2.70 (m, 2H, H-4a), 0.91-0.87 (m, 3H, CH_3). **Chromane:** δ 7.28-7.17 (m, 1H, H-7), 6.92-6.89 (m, 1H, H-5), 6.85-6.81 (m, 1H, H-6), 6.72-6.69 (m, 1H, H-8), 6.02 (dd, $^1J_{H-H}$ = 12 Hz $^2J_{H-H}$ = 6 Hz, 1H, H-4), 2.43 (dd, $^1J_{H-H}$ = 13 Hz $^2J_{H-H}$ = 6.5 Hz, 1H, H-3a), 2.20-2.17 (m, 1H, H-3a'), 1.87-1.28 (m, 20H, 10CH_2). RMN ^{13}C (100MHz, $CDCl_3$) **Triazole:** δ 149.0 (C-4), 118.7 (C-5), 25.8 (C-4a), 14.0 (CH_3). **Chromane:** δ 153.6 (C-8a), 129.9 (C-7), 127.3 (C-8), 120.5 (C-6), 119.6 (C-4a), 118.0 (C-5), 80.5 (C-2), 54.1 (C-4), 41.5 (C-3), 41.0 (CH_2), 35.5 (CH_2), 31.5 (CH_2), 29.7 (CH_2), 29.6 (CH_2), 29.3 (CH_2), 28.8 (CH_2), 25.8 (CH_2), 22.5 (CH_2), 22.1 (CH_2), 21.8 (CH_2). HRMS: Calcd. $C_{22}H_{33}N_3O_2$: 368.2696. Exp: 368.2701.

Acknowledgements

The authors would like to thank: Coordination for Improvement of Higher Education Personnel (CAPES) for the fellowships; and the National Council for Scientific and Technological Development (CNPq) (Proc. numbers 306.883/2015-5 and 402.075/2016-1, CNPq/Universal) and the Research Support Foundation of the State of Rio Grande do Sul (FAPERGS) (PqG, proc. number 17/2551-0001275-5) for the financial support. Bernardo A. Iglesias thanks Conselho Nacional de Desenvolvimento Científico e Tecnológico (CNPq – Brazil; Universal process 409150/2018-5 and PG-2018 grants process 304711/2018-7) and CAPES/PROEX – Finance Code 001.

Declaration of Interest Statement

The authors declare no conflict of interest

Conflict of Interest

The authors declare no conflict of interest.

References

[1] A. Rani, G. Singh, A. Singh, U. Maqbool, G. Kaur, J. Singh, CuAAC-ensembled 1,2,3-triazole-linked isosteres as pharmacophores in drug discovery: Review, RSC Adv. 10 (2020) 5610–5635. doi:10.1039/c9ra09510a.

[2] K. Bozorov, J. Zhao, H.A. Aisa, 1,2,3-Triazole-containing hybrids as leads in medicinal chemistry: A recent overview, Bioorganic Med. Chem. 27 (2019) 3511–3531. doi:10.1016/j.bmc.2019.07.005.

[3] W. Fan, A.R. Katritzky, 1,2,3-Triazoles, in: Compr. Heterocycl. Chem. II, Pergamon P, Oxford., 1996: p. 1–1003. https://www.elsevier.com/books/comprehensive-heterocyclic-chemistry-iii/katritzky/978-0-08-044991-3.

[4] V. V Rostovtsev, L.G. Green, V. V Fokin, K.B. Sharpless, A stepwise huisgen cycloaddition process: Copper(I)-catalyzed regioselective "ligation" of azides and terminal alkynes, Angew. Chemie - Int. Ed. 41 (2002) 2596–2599. doi:10.1002/1521-3773(20020715)41:14<2596::AID-ANIE2596>3.0.CO;2-4.

[5] C.W. Tornøe, C. Christensen, M. Meldal, Peptidotriazoles on solid phase:

[1,2,3]-Triazoles by regiospecific copper(I)-catalyzed 1,3-dipolar cycloadditions of terminal alkynes to azides, J. Org. Chem. 67 (2002) 3057–3064. doi:10.1021/jo011148j.

[6] B.T. Worrell, J.A. Malik, V. V. Fokin, Direct evidence of a dinuclear copper intermediate in Cu(I)-catalyzed azide-alkyne cycloadditions, Science (80-.). 340 (2013) 457–460. doi:10.1126/science.1229506.

[7] K. Lal, C.P. Kaushik, A. Kumar, CHEMISTRY Antimicrobial evaluation , QSAR and docking studies, Med. Chem. Res. 24 (2015) 3258–3271. doi:10.1007/s00044-015-1378-9.

[8] F. de C. da Silva, M.C.B.V. de Souza, I.I.P. Frugulhetti, H.C. Castro, S.L. d. O. Souza, T.M.L. de Souza, D.Q. Rodrigues, A.M.T. Souza, P.A. Abreu, F. Passamani, C.R. Rodrigues, V.F. Ferreira, Synthesis, HIV-RT inhibitory activity and SAR of 1-benzyl-1H-1,2,3-triazole derivatives of carbohydrates, Eur. J. Med. Chem. 44 (2009) 373–383. doi:10.1016/j.ejmech.2008.02.047.

[9] W. Zhang, Z. Li, M. Zhou, F. Wu, X. Hou, H. Luo, H. Liu, X. Han, G. Yan, Z. Ding, R. Li, Bioorganic & Medicinal Chemistry Letters derivatives as potential antitumor agents, Bioorg. Med. Chem. Lett. 24 (2014) 799–807. doi:10.1016/j.bmcl.2013.12.095.

[10] A. Kishore Kumar, V. Sunitha, B. Shankar, M. Ramesh, T. Murali Krishna, P. Jalapathi, Synthesis, biological evaluation, and molecular docking studies of novel 1,2,3-triazole derivatives as potent anti-inflammatory agents, Russ. J. Gen. Chem. 86 (2016) 1154–1162. doi:10.1134/S1070363216050297.

[11] Y. Sajja, S. Vanguru, L. Jilla, H. Reddy, R. Bantu, Bioorganic & Medicinal Chemistry Letters, A convenient synthesis and screening of benzosuberone bearing, Bioorg. Med. Chem. Lett. 26 (2016) 4292–4295. doi:10.1016/j.bmcl.2016.07.039.

[12] D. Ashok, P. Chiranjeevi, A.V. Kumar, M. Sarasija, V.S. Krishna, D. Sriram, S. Balasubramanian, 1,2,3-Triazole-fused spirochromenes as potential anti-tubercular agents: synthesis and biological evaluation, RSC Adv. 8 (2018) 16997–17007. doi:10.1039/c8ra03197e.

[13] L. Feng, M.M. Maddox, M.Z. Alam, L.S. Tsutsumi, G. Narula, D.F. Bruhn, X. Wu, S. Sandhaus, R.B. Lee, C.J. Simmons, Y.C. Tse-Dinh, J.G. Hurdle, R.E. Lee, D. Sun, Synthesis, structure-activity relationship studies, and antibacterial

evaluation of 4-chromanones and chalcones, as well as olympicin A and derivatives, J. Med. Chem. 57 (2014) 8398–8420. doi:10.1021/jm500853v.

[14] R.R. Dandu, J.A. Lyons, R. Raddatz, Z. Huang, L.D. Aimone, R.L. Hudkins, Bioorganic & Medicinal Chemistry Letters Synthesis and evaluation of a new series of 10-cyclobutyl-6-(4-piperidyloxy)spiro[benzopyran-2,40-piperidine] derivatives as high affinity and selective histamine-3 receptor (H3R) antagonists, Bioorg. Med. Chem. Lett. 22 (2012) 2151–2153. doi:10.1016/j.bmcl.2012.01.139.

[15] T. Huang, J. Sun, Q. Wang, J. Gao, Y. Liu, Synthesis, biological evaluation and molecular docking studies of piperidinylpiperidines and spirochromanones possessing quinoline moieties as Acetyl-CoA carboxylase inhibitors, Molecules. 20 (2015) 16221–16234. doi:10.3390/molecules200916221.

[16] E.O. Meltzer, Intranasal steroids: Managing allergic rhinitis and tailoring treatment to patient preference, Allergy Asthma Proc. 26 (2005) 445–451.

[17] D. Ashok, D. Mohan, G. Aamate, V. Kumar, CHEMISTRY Microwave assisted synthesis, biological evaluation and molecular docking of novel chroman scaffolds incorporating spirochromanone framework, Med. Chem. Res. 25 (2016) 2882–2894. doi:10.1007/s00044-016-1699-3.

[18] N.R. Kishore, D. Ashok, M. Sarasija, N.Y.S. Murthy, One-pot synthesis of spirochromanone-based 3-hydroxy-4H-chromen-4-ones by a modified Algar–Flynn–Oyamada reaction and evaluation of their antimicrobial activity, Chem. Heterocycl. Compd. 53 (2017) 1187–1191. doi:10.1007/s10593-018-2200-7.

[19] S.A. Abdelatef, M.I. El-saadi, N.H. Amin, A.H. Abdelazeem, H.A. Omar, K.R.A. Abdellatif, European Journal of Medicinal Chemistry Design, Synthesis and anticancer evaluation of novel spirobenzo[h]chromene and spirochromane derivatives with dual EGFR and B-RAF inhibitory activities, Eur. J. Med. Chem. 150 (2018) 567–578. doi:10.1016/j.ejmech.2018.03.001.

[20] H.G. Bonacorso, L.B. Silva, J.B.T. Rocha, P.A. Nogara, E.P. Waczuk, F.D.A. Silva, D.C. Bueno, Y.N.A.M. Kader, M.A.P. Martins, N. Zanatta, Synthesis , biological evaluation and molecular docking study of 7- tacrine hybrids, Tetrahedron Lett. 56 (2015) 7024–7027. doi:10.1016/j.tetlet.2015.11.008.

[21] H.G. Bonacorso, P.T. Campos, L.B. Silva, B.A. Iglesias, N. Zanatta, M. Hörner, Structural Investigation , UV – Vis Analysis and Crystal Packing Tacrine

Hybrids by Single Crystal X-Ray Diffraction, J. Chem. Crystallogr. 48 (2018) 19–31. doi:10.1007/s10870-018-0706-6.

[22] F. Costa, L. Barros, E. Winter, A. Henrique, L. João, D. Melo, M. Rode, M. Antônio, P. Martins, N. Zanatta, BBA - General Subjects Tacrine derivatives stimulate human glioma SF295 cell death and alter important proteins related to disease development : An old drug for new targets, BBA - Gen. Subj. 1862 (2018) 1527–1536. doi:10.1016/j.bbagen.2018.04.019.

[23] M. Muthukrishnan, M. Mujahid, P. Yogeeswari, D. Sriram, Syntheses and biological evaluation of new triazole-spirochromone conjugates as inhibitors of Mycobacterium tuberculosis, Tetrahedron Lett. 52 (2011) 2387–2389. doi:10.1016/j.tetlet.2011.02.099.

[24] M. Mujahid, R.G. Gonnade, P. Yogeeswari, D. Sriram, M. Muthukrishnan, Bioorganic & Medicinal Chemistry Letters Synthesis and antitubercular activity of amino alcohol fused spirochromone conjugates, Bioorg. Med. Chem. Lett. 23 (2013) 1416–1419. doi:10.1016/j.bmcl.2012.12.073.

[25] H.J. Kabbe, Eine einfache Synthese von 4-Chromanonen, Synthesis (Stuttg). 2 (1978) 886–887. doi:10.1017/CBO9781107415324.004.

[26] H.G. Bonacorso, A. Ketzer, W.C. Rosa, T.P. Calheiro, M.B. Rodrigues, N. Zanatta, M.A.P. Martins, C.M. Frizzo, Useful approach for O-functionalization of trifluoromethyl-substituted spirotetracyclic isoxazolines, and their application in the synthesis of 1,2,3-triazole derivatives, J. Fluor. Chem. 210 (2018) 142–148. doi:10.1016/j.jfluchem.2018.03.012.

[27] F. Connors, R.V., Kang, D., John, E., Pingchen, F., Benjamin, F. Jiasheng, GEM-DISUBSTITUTED AND SPIROCYCLIC AMINO PYRIDINES/PYRIMIDINES AS CELL CYCLE INHIBITORS, WO/2009/126584, 2009. https://patentscope.wipo.int/search/en/detail.jsf?docId=WO2009126584.

[28] M. Kavala, F. Mathia, J. Kožíšek, P. Szolcsányi, Efficient total synthesis of (+)-dihydropinidine, (-)-epidihydropinidine, and (-)-pinidinone, J. Nat. Prod. 74 (2011) 803–808. doi:10.1021/np100852p.

[29] J.E. Hein, V. V Fokin, Copper-catalyzed azide-alkyne cycloaddition (CuAAC) and beyond: New reactivity of copper(I) acetylides, Chem. Soc. Rev. 39 (2010) 1302–1315. doi:10.1039/b904091a.

[30] H.C. Kolb, M.G. Finn, K.B. Sharpless, Click Chemistry: Diverse Chemical Function from a Few Good Reactions, Angew. Chemie - Int. Ed. 40 (2001) 2004–2021. doi:10.1002/1521-3773(20010601)40:11<2004::AID-ANIE2004>3.0.CO;2-5.

[31] P. Müller, R. Herbst-Irmer, A.L. Spek, T.R. Schneider, M.R. Sawaya, Crystal Structure Refinement: A Crystallographer's Guide to SHELXL, Oxford University Press, 2010. doi:10.1093/acprof:oso/9780198570769.001.0001.

[32] T. Aravinda, H.S. Bhojya Naik, H.R. Prakash Naik, 1,2,3-triazole fused quinoline-peptidomimetics: Studies on synthesis, DNA binding and photonuclease activity, Int. J. Pept. Res. Ther. 15 (2009) 273–279. doi:10.1007/s10989-009-9188-x.

[33] O.A. Chaves, T.P. Calheiro, J.C. Netto-Ferreira, M.C.C. de Oliveira, S.Z. Franceschini, C.M.C. de Salles, N. Zanatta, C.P. Frizzo, B.A. Iglesias, H.G. Bonacorso, Biological assays of BF_2-naphthyridine compounds: Tyrosinase and acetylcholinesterase activity, CT-DNA and HSA binding property evaluations, Int. J. Biol. Macromol. 160 (2020) 1114–1129. doi:10.1016/j.ijbiomac.2020.05.162.

[34] H. Isobe, T. Fujino, Triazole-linked analogues of DNA and RNA (TLDNA and TLRNA): Synthesis and functions, Chem. Rec. 14 (2014) 41–51. doi:10.1002/tcr.201300023.

[35] F. Zhao, X. Sun, W. Lu, L. Xu, J. Shi, S. Yang, M. Zhou, F. Su, F. Lin, F. Cao, Synthesis of novel, DNA binding heterocyclic dehydroabietylamine derivatives as potential antiproliferative and apoptosis-inducing agents, Drug Deliv. 27 (2020) 216–227. doi:10.1080/10717544.2020.1716879.

[36] A. Paul, P. Guo, D.W. Boykin, W.D. Wilson, A new generation of minor-groove-binding—heterocyclic diamidines that recognize G·C base pairs in an at sequence context, Molecules. 24 (2019) 946. doi:10.3390/molecules24050946.

[37] O. Augusto, T. Vinício, A. Fernandes, J. Luiz, R. De Melos, J.C. Netto-ferreira, A. Echevarria, Elucidation of the interaction between human serum albumin (HSA) and potential drug for Leishmania amazonensis : Multiple spectroscopic and dynamics simulation approach, J. Mol. Liq. 310 (2020) 1–9. doi:10.1016/j.molliq.2020.113117.

[38] M.E.F. Franklim, T. N., Freire-de-Lima, L., Chaves, O. A., LaRocque-de-Freitas,

I. F., da Silva-Trindade, J. D., Netto-Ferreira, J. C., Freire-de-Lima, C. G., Decoté-Ricardo, D., Previato, J. O., Mendonça-Previato, L., de Lima, Design, Synthesis, Trypanocidal Activity, and Studies on Human Albumin Interaction of Novel S-Alkyl-1,2,4-triazoles, J. Braz. Chem. Soc. 30 (2019) 1378–1394.

[39] O. Augusto, L. Santos, D. Barros, M.C.C. De Oliveira, C. Mauricio, R.S. Anna, A.B.B. Ferreira, F. Assis, D. Cesarin-sobrinho, J.C. Netto-ferreira, Biological interactions of fl uorinated chalcones : Stimulation of tyrosinase activity and binding to bovine serum albumin, J. Fluor. Chem. 199 (2017) 30–38. doi:10.1016/j.jfluchem.2017.04.007.

[40] O.A. Chaves, C.S.H. Jesus, P.F. Cruz, C.M.R. Sant'Anna, R.M.M. Brito, C. Serpa, Evaluation by fluorescence, STD-NMR, docking and semi-empirical calculations of the o-NBA photo-acid interaction with BSA, Spectrochim. Acta - Part A Mol. Biomol. Spectrosc. 169 (2016) 175–181. doi:10.1016/j.saa.2016.06.028.

[41] P.R.S. Salbego, T. Orlando, F.F.S. Farias, H.G. Bonacorso, M.A.P. Martins, [2]Rotaxanes Bearing a Tetralactam Macrocycle: The Role of a Trifurcated Hydrogen Bond in the Crystalline State, European J. Org. Chem. 2019 (2019) 3464–3471. doi:10.1002/ejoc.201900216.

[42] R.F.W. Bader, Atoms in Molecules: A Quantum Theory, Oxford University Press, Oxford, U.K., 1990.

[43] R.F.W. Bader, A quantum theory of molecular structure and its applications, Chem. Rev. 91 (1991) 893–928. doi:10.1021/cr00005a013.

[44] J.S. Murray, P. Politzer, The electrostatic potential: An overview, Wiley Interdiscip. Rev. Comput. Mol. Sci. 1 (2011) 153–163. doi:10.1002/wcms.19.

[45] M.H. Kolář, P. Hobza, Computer Modeling of Halogen Bonds and Other σ-Hole Interactions, Chem. Rev. 116 (2016) 5155–5187. doi:10.1021/acs.chemrev.5b00560.

[46] R. Santosh, M.K. Selvam, S.U. Kanekar, G.K. Nagaraja, M. Kumar, Design, Synthesis, DNA Binding, and Docking Studies of Thiazoles and Thiazole-Containing Triazoles as Antibacterials, ChemistrySelect. 3 (2018) 3892–3898. doi:10.1002/slct.201800222.

[47] K. Ekambareswara Rao, K. Krowicki, G. Burckhardt, C. Zimmer, J.W. Lown, Molecular Recognition between Oligopeptides and Nucleic Acids: DNA Binding

Selectivity of a Series of 1,2,4-Triazole-Containing Lexitropsins, Chem. Res. Toxicol. 4 (1991) 241–252. doi:10.1021/tx00020a019.

[48] A. Wolfe, G.H.S. Jr, T. Meehan, Polycyclic aromatic hydrocarbons physically intercalate into duplex regions of denatured DNA Polycyclic Aromatic Hydrocarbons Physically Intercalate into Duplex Regions of Denatured DNA, Biochemistry. 26 (1987) 6392–6396. doi:10.1021/bi00394a013.

[49] J.C.P. Mayer, A.C. Sauer, B.A. Iglesias, T. V. Acunha, D.F. Back, O.E.D. Rodrigues, L. Dornelles, Ferrocenylethenyl-substituted 1,3,4-oxadiazolyl-1,2,4-oxadiazoles: Synthesis, characterization and DNA-binding assays, J. Organomet. Chem. 841 (2017) 1–11. doi:10.1016/j.jorganchem.2017.04.014.

[50] M.R. Eftink, C.A. Ghiron, Fluorescence quenching studies with proteins, Anal. Biochem. 114 (1981) 199–227. doi:10.1016/0003-2697(81)90474-7.

[51] M.B. Rodrigues, S.C. Feitosa, C.W. Wiethan, W.C. Rosa, C.H. da Silveira, A.B. Pagliari, M.A.P. Martins, N. Zanatta, B.A. Iglesias, H.G. Bonacorso, Ullmann-type copper-catalyzed coupling amination, photophysical and DNA/HSA-binding properties of new 4-(trifluoromethyl)quinoline derivatives, J. Fluor. Chem. 221 (2019) 84–90. doi:10.1016/j.jfluchem.2019.04.006.

[52] N.A. Durandin, V.B. Tsvetkov, E.E. Bykov, D.N. Kaluzhny, S.N. Lavrenov, A.N. Tevyashova, M.N. Preobrazhenskaya, Quantitative parameters of complexes of tris(1-alkylindol-3-yl)methylium salts with serum albumin: Relevance for the design of drug candidates, J. Photochem. Photobiol. B Biol. 162 (2016) 570–576. doi:10.1016/j.jphotobiol.2016.07.017.

[53] A. Hemamalini, E.R. Azhagiya Singam, S.K. Mudedla, V. Subramanian, T. Mohan Das, Design and synthesis of sugar-triazole based uracil appended sugar-imine derivatives-an application in DNA binding studies, New J. Chem. 39 (2015) 4575–4582. doi:10.1039/c4nj02221a.

[54] D.S. Saini K.S., Ashraf R., Mandalapu D., Das S., Siddiqui M.Q., New Orally Active DNA Minor Groove Binding Small Molecule CT-1 Acts Against Breast Cancer by Targeting Tumor DNA Damage Leading to p53-Dependent Apoptosis, Mol Carcinog. 54 (2017) 1266–1280.

[55] J. Li, H. Feng, R. Liu, G. Ding, H. Si, W. He, Z. Sun, The computational and experimental studies on a 1, 2, 3-triazole compound and its special binding to three kinds of blood proteins, J. Biomol. Struct. Dyn. 38 (2020) 1185–1196.

doi:10.1080/07391102.2019.1598498.

[56] A.S.K. Sharma K., Yadav P., Sharma B., Pandey M., Interaction of coumarin triazole analogs to serum albumins: Spectroscopic analysis and molecular docking studies., J Mol Recognit. 33 (2020) 2834.

[57] S.K. Maddili, R. Katla, V.K. Kannekanti, N.K. Bejjanki, B. Tuniki, C.H. Zhou, H. Gandham, Molecular interaction of novel benzothiazolyl triazolium analogues with calf thymus DNA and HSA-their biological investigation as potent antimicrobial agents, Eur. J. Med. Chem. 150 (2018) 228–247. doi:10.1016/j.ejmech.2018.02.056.

[58] P. Ascenzi, A. di Masi, G. Fanali, M. Fasano, Heme-based catalytic properties of human serum albumin, Cell Death Discov. 1 (2015) 1–7. doi:10.1038/cddiscovery.2015.25.

[59] G.M. Sheldrick, A short history of SHELX, Acta Cryst. A64 (2008) 112–122. doi:10.1107/S0108767307043930.

[60] L.J. Bourhis, O. V. Dolomanov, R.J. Gildea, J.A.K. Howard, H. Puschmann, The anatomy of a comprehensive constrained, restrained refinement program for the modern computing environment – Olex2 dissected, Acta Crystallogr. Sect. A Found. Adv. 71 (2015) 59–75. doi:10.1107/S2053273314022207.

[61] G.M. Sheldrick, Crystal structure refinement with SHELXL, Acta Crystallogr. Sect. C Struct. Chem. 71 (2015) 3–8. doi:10.1107/S2053229614024218.

[62] O. V. Dolomanov, L.J. Bourhis, R.J. Gildea, J.A.K. Howard, H. Puschmann, OLEX2 : a complete structure solution, refinement and analysis program, J. Appl. Crystallogr. 42 (2009) 339–341. doi:10.1107/S0021889808042726.

[63] Cambridge Crystallographic Data Centre, Mercury CSD Version 4.3.1, CCDC, Cambridge, U.K., 2020.

[64] M.J. Frisch, G.W. Trucks, H.B. Schlegel, G.E. Scuseria, M.A. Robb, J.R. Cheeseman, G. Scalmani, V. Barone, G.A. Petersson, H. Nakatsuji, X. Li, M. Caricato, A. Marenich, J. Bloino, B.G. Janesko, R. Gomperts, B. Mennucci, H.P. Hratchian, J. V. Ortiz, A.F. Izmaylov, J.L. Sonnenberg, D. Williams-Young, F. Ding, F. Lipparini, F. Egidi, J. Goings, B. Peng, A. Petrone, T. Henderson, D. Ranasinghe, V.G. Zakrzewski, N.R. J. Gao, G. Zheng, W. Liang, M. Hada, M. Ehara, K. Toyota, R. Fukuda, J. Hasegawa, M. Ishida, T. Nakajima, Y. Honda, O. Kitao, H. Nakai, T. Vreven, K. Throssell, J.A.J. Montgomery, J.E. Peralta, F.

Ogliaro, M. Bearpark, J.J. Heyd, E. Brothers, K.N. Kudin, V.N. Staroverov, T. Keith, R. Kobayashi, J. Normand, K. Raghavachari, A. Rendell, J.C. Burant, S.S. Iyengar, J. Tomasi, M. Cossi, J.M. Millam, M. Klene, C. Adamo, R. Cammi, J.W. Ochterski, R.L. Martin, K. Morokuma, O. Farkas, J.B. Foresman, D.J. Fox, Gaussian 09, Revision C.01., Gaussian, Inc, Wallingford, CT, 2010.

[65] S.F. Boys, F. Bernardi, The calculation of small molecular interactions by the differences of separate total energies. Some procedures with reduced errors, Mol. Phys. 19 (1970) 553–566. doi:10.1080/00268977000101561.

[66] T.A. Keith, AIMAll Version 14.11.23, TK Gristmill Software, Overland Park, KS, 2014.

[67] H.P. Hratchian, T.A. Keith, J. Millam, Gaussian 09 User's Reference, Semichem Inc.: Shawnee Mission, KS, 2009.

[68] D.P. Heller, C.L. Greenstock, Fluorescence lifetime analysis of DNA intercalated ethidium bromide and quenching by free dye, Biophys. Chem. 50 (1994) 305–312. doi:10.1016/0301-4622(93)E0101-A.

[69] A.K. Estandarte, S. Botchway, C. Lynch, M. Yusuf, I. Robinson, The use of DAPI fluorescence lifetime imaging for investigating chromatin condensation in human chromosomes, Sci. Rep. 6 (2016) 1–12. doi:10.1038/srep31417.

[70] O.A. Chaves, T. V. Acunha, B.A. Iglesias, C.S.H. Jesus, C. Serpa, Effect of peripheral platinum(II) bipyridyl complexes on the interaction of tetra-cationic porphyrins with human serum albumin, J. Mol. Liq. 301 (2020) 112466. doi:10.1016/j.molliq.2020.112466.

[71] O. Trott, A.J. Olson, AutoDock Vina: Improving the Speed and Accuracy of Docking with a New Scoring Function, Efficient Optimization, and Multithreading, J. Comput. Chem. 31 (2010) 455–461. doi:10.1002/jcc.21334.

[72] H.R. Drew, R.M. Wing, T. Takano, C. Broka, S. Tanaka, K. Itakura, R.E. Dickerson, Structure of a B-DNA dodecamer: conformation and dynamics, Proc. Natl. Acad. Sci. 78 (1991) 2179–2183. doi:10.1073/pnas.78.4.2179.

[73] L. Zhu, F. Yang, L. Chen, E.J. Meehan, M. Huang, A new drug binding subsite on human serum albumin and drug–drug interaction studied by X-ray crystallography, J. Struct. Biol. 162 (2008) 40–49. doi:10.1016/j.jsb.2007.12.004.

[74] E.F. Pettersen, T.D. Goddard, C.C. Huang, G.S. Couch, D.M. Greenblatt, E.C. Meng, T.E. Ferrin, UCSF Chimera - A visualization system for exploratory

research and analysis, J. Comput. Chem. 25 (2004) 1605–1612. doi:10.1002/jcc.20084.

[75] M.D. Hanwell, D.E. Curtis, D.C. Lonie, T. Vandermeersch, E. Zurek, G.R. Hutchison, Avogadro: an advanced semantic chemical editor, visualization, and analysis platform, J. Cheminform. 4 (2012) 1–17. doi:10.1186/1758-2946-4-17.

[76] J.J.P. Stewart, Optimization of parameters for semiempirical methods V: Modification of NDDO approximations and application to 70 elements, J. Mol. Model. 13 (2007) 1173–1213. doi:10.1007/s00894-007-0233-4.

[77] J.J.P. Stewart, MOPAC, (2016).

[78] G.M. Morris, R. Huey, W. Lindstrom, M.F. Sanner, R.K. Belew, D.S. Goodsell, A.J. Olson, AutoDock4 and AutoDockTools4: Automated Docking with Selective Receptor Flexibility, J. Comput. Chem. 30 (2009) 2785–2791. doi:10.1002/jcc.21256.

[79] Dassault Systèmes BIOVIA, Accelrys Discovery Studio Visualizer, (2017).

Graphical Abstract

Highlights

- *Click Chemistry was successful employed to obtain novel spiro[chroman-2,1'-cycloalkanyl]-1*H*-1,2,3-triazole scaffolds.
- *Derivatives interact strongly in the minor groove of CT-DNA via ground-state association.
- * SC-XRD data for SCT1 enabled a broad molecular insight using QTAIM and MEP analysis.